STRAIN VARIATION BETWEEN THE MONTEREY AND SISQUOC FORMATIONS, SOUTHERN SANTA MARIA BASIN, CALIFORNIA, USA: IMPLICATIONS FOR STRUCTURAL ASSESSMENT OF FOLD AND THRUST BELTS

A THESIS

Presented to the Department of Geological Sciences

California State University, Long Beach

In Partial Fulfillment

of the Requirements for the Degree

Master of Science in Geology

Committee Members:

Richard J. Behl, Ph.D., (Chair)
Nate W. Onderdonk, Ph.D. (Chair)
Thomas L. Davis, Ph.D.
Jay S. Namson, Ph.D.

College Designee:

Richard J. Behl, Ph.D.

By Yannick Wirtz

B.S., 2013, RWTH Aachen University of Technology, Aachen, Germany

August 2017

ABSTRACT

STRAIN VARIATION BETWEEN THE MONTEREY AND SISQUOC FORMATIONS, SOUTHERN SANTA MARIA BASIN, CALIFORNIA, USA: IMPLICATIONS FOR STRUCTURAL ASSESSMENT OF FOLD AND THRUST BELTS

By

Yannick Wirtz

August 2017

Analysis of variation of fold strain at map-scale and outcrop-scale of the siliceous Monterey and Sisquoc formations in the southern Santa Maria basin, California provides insight into limitations of strain determination by construction of area-conservative balanced cross-sections. Diagenetic modification of these rocks allows strain quantification of rock intervals with high competence contrasts. Detailed strain analysis at map-scale shows significant variation in fold strain between rock types with shortening values ranging from 5.5 % to 21.1 %. Apparent shortening in the competent Monterey Formation is twice as high as in the overlying highly porous Sisquoc Formation. The large difference in apparent shortening suggests that the same amount of actual strain was accommodated by folding in the Monterey and horizontal compaction in the Sisquoc Formation, since there is no evidence of a detachment fault or major unconformity between the units. Strain analysis at outcrop-scale provides insight into how both units express such different shortening ratios without having an unconformity, or detachment fault between them.

ACKNOWLEDGEMENTS

Thank you to everyone who supported me throughout this thesis project.

To Dr. Richard Behl and Dr. Nate Onderdonk for giving me the opportunity to be your graduate student and study under perfect work conditions at California State University, Long Beach. Dr. Behl, I am more than grateful for being a part of your Monterey and Related Sediments (MARS) research group. Your guidance in approaching, communicating, and presenting this thesis project was invaluable to my education.

To Thom Davis and Jay Namson for the critical input, technical advice, and software training in structural geology. Thank you for giving me the chance to contribute this research to your professional field trips, teaching me on your incredible knowledge in California structural geology, and supporting me in so many ways.

To Stefano Mazzoni for helping me get started on the critical software that was used for this thesis project.

To Earth Consultants International for providing field gear, cameras, and critical software. A special thank you to Anders Hogrelius for helping to collect data in the field.

To Margaret Costello and Dan Pankratz for your help keeping the CSULB geology department running smoothly.

To my CSULB friends Ryan Stewart, Maia Davis, Ryan Weller, Brendan Neel, Jack Farrell, AJ White, and Tom Kelty for all their support.

To my Dad. Without his help, it would have been impossible to study abroad.

TABLE OF CONTENTS

ABSTRACT ii

ACKNOWLEDGEMENTS iii

LIST OF TABLES v

LIST OF FIGURES vi

1. INTRODUCTION 1
2. GEOLOGIC SETTING 3
3. MAP-SCALE STRAIN ANALYSIS 21
4. OUTCROP-SCALE STRAIN ANALYSIS 39
5. DISCUSSION 47
6. CONCLUSION 62

APPENDIX: CONSTRUCTED CROSS-SECTIONS USED FOR STRAIN QUANTIFICATION IN THE LOMPOC - SANTA ROSA FOLD BELT AND LOMPOC - PURISIMA ANTICLINE FOLD BELT 64

REFERENCES 72

LIST OF TABLES

1. Map-Scale Strain Analysis Results 29
2. Results for Measured Fold Angles in the Sisquoc and Monterey Formations 33
3. Slope Function for Wavelength vs. Amplitude for the LSR and LPA 35
4. Slope Function for Amplitude vs. Wavelength for the LSR and LPA 38

LIST OF FIGURES

1. Regional geologic setting of the Santa Maria basin area showing location of study area 4

2. Interpretive kinematic reconstruction of southern and central California from 19 Ma to present based on paleomagnetic data 5

3. Regional balanced cross-section across the Santa Maria basin 8

4. Strain partitioning model showing transpression along the San Andreas active plate margin is resolved into two components 10

5. Physiographic setting and boundaries of study areas 12

6. Geologic map of the southern Santa Maria basin showing the two study areas: Lompoc-Purisima-Anticline (LPA) fold belt to the north, and the Lompoc-Santa Rosa (LSR) fold belt to the south 13

7. Silica phase changes during diagenesis and associated lithologies and stepped changes in porosity with depth 17

8. Sketch of diagenetic modification of a representative section in the upper Monterey Formation. 18

9. Locations of line-length-sections created in this study, and location of outcrop-scale structural analysis at Sweeney Road and San Miguelito Canyon 23

10. Construction method of line-length-sections 25

11. Schematic line-length-section showing different section components used for shortening calculations and fold geometry analyses 26

12. Histogram of fold shortening estimates in the LSR and LPA 31

13. Correlation of the formational ratio (Sisquoc : Monterey) used during line-length-section construction over shortening results in LSR (orange) and LPA (blue) 32

14. Histogram of fold angles measured in the Sisquoc and Monterey formations for the LSR and LPA 34

15. Correlation of fold wavelength against fold amplitude for the Sisquoc Formation and Monterey Formation folds in the LSR and LPA 36

16. Correlation of fold amplitude against fold shortening in the Sisquoc Formation and Monterey Formation folds in the LSR and LPA 37

17. Image of a well-exposed and deformed section of the upper Monterey Formation at San Miguelito Canyon 40

18. Image of Sweeney Road section and orthoimage that was used for outcrop-scale structural analysis 42

19. Map of fold structures in the Sisquoc Formation and upper Monterey Formation at Sweeney Road 43

20. Generalized geologic map and interpretation of deformation mechanisms in the Monterey and Sisquoc formations 50

21. Tectonic wedge model tying the regional cross section by Namson and Davis (1990) with sub regional-scale deformation in the Monterey and Sisquoc formations observed and measured in this study 60

CHAPTER 1

INTRODUCTION

The reconstruction of the geometric and kinematic evolution of fold-and-thrust belts requires depiction of deformation mechanisms and quantification of shortening. Depending on scale and method, this can be done by measuring the contraction resulting from mechanisms including the net slip on thrust faults (translation), the amount of folding (horizontal rotation) and layer-parallel shortening (pure strain) (Fossen, 2016). Balanced cross-sections account for translational and rotational components and perform one- or two-dimensional strain analyses by integrating surface and subsurface data across fold-and-thrust belts generally at regional scales. The construction of these sections produces geometric and kinematic models, illustrates the deformational history, and predicts structural traps for petroleum prospects in basin exploration (Dahlstrom, 1970; Suppe, 1980; Namson and Davis, 1988 a, 1988b; Mitra and Namson, 1989; Namson and Davis, 1990). Yet, balanced cross-sections have limitations because they do not account for the different mechanical behaviors of rocks and their deformation mechanisms at more detailed scales that may affect geometric and kinematic expression of strain in fold-and-thrust belts.

It has been shown that by focusing on particular scales, lithologies, and environmental conditions (e.g., pressure, temperature), significant differences can arise with respect to the deformational pattern (Snyder et al., 1983; Behl, 1992; Gross and Engelder, 1995; Fischer and Jackson, 1999), the amount of shortening (Cooper, 1983; Smart et al., 1997; Hogan and Dunne, 2001; Duebendorfer and Meyer, 2002; Koyi et al., 2003), the variation in strain and structural style along strike (Onderdonk, 2005; Carbonell et al., 2013), and interpretation of the kinematics and mechanics of emplacement of thrusts (Mitra, 1994; Mukul, 1999; McQuarrie and Davis,

2002). Therefore, strain information derived from different scales and lithologies of contrasting physical properties may significantly improve our understanding of the structural style and kinematic evolution of fold-and-thrust belts.

Siliceous sedimentary rocks can exhibit very heterogeneous and contrasting physical properties. Mesozoic and Cenozoic siliceous sedimentary basin deposits are widespread around the world, including circum-Pacific orogenic belts in coastal California, Mexico, and Japan; the North Sea, the southwest Indian ridge, and the calcareous Alps (Hein and Parrish, 1987). The initial composition of siliceous sediments are highly porous oozes of diatoms or radiolarians before undergoing significant and complex mechanical modification with burial diagenesis resulting in variations in physical rock properties (Isaacs, 1981). This opens up the opportunity to study the magnitude of strain variation across mechanically contrasting lithologies in fold-and-thrust belts at map-scale and outcrop-scale.

This study quantifies and analyzes the variation of strain of the petroliferous Monterey and Sisquoc formations in the southern Santa Maria basin, California, USA, because they comprise siliceous strata of a distinct diagenetic stage. The study area is located in a complicated tectonic setting along a transpressional active plate margin where depiction of deformation mechanisms is important to better understand the kinematic evolution of the plate margin. This work provides an explanation for how distinct deformational styles between competence-contrasting siliceous diagenetic rocks at formational- and outcrop-scale can exist without a detachment fault between them, and opens up new possibilities for geometric and kinematic interpretations of the southern Santa Maria basin tectonic province.

CHAPTER 2

GEOLOGIC SETTING

Regional Geology

The Santa Maria basin (SMB) of California, USA is a Neogene petroleum basin located at the junction of two tectonic provinces: the northwest-southeast trending Coast Ranges, and the east-west trending Transverse Ranges. The triangular basin is structurally bounded by the Santa Maria River - Foxen Canyon - Little Pine fault zone to the northeast, the Santa Ynez fault zone to the south, and the offshore Hosgri fault zone to the west. Structures internal to the basin, including folds and faults, have westerly to northwesterly trends (Fig. 1).

The SMB is one of several coastal California basins, including the Los Angeles, the Ventura - Santa Barbara, the Pismo – Huasna, and the Salinas basins that formed during Miocene to Pliocene time when the boundary between the Pacific and North American plates shifted from a convergent to a transform setting (Blake et al., 1978; Ingersoll and Ernst, 1987). The kinematics of coastal California basin development are interpreted to be differential translation and rotation motions of large crustal blocks during diffuse shear along the San Andreas fault system from middle Miocene to present (Fig. 2) (Luyendyk and Hornafius, 1987; Nicholson et al., 1994; McCrory et al., 1995). This interpretation is mainly based on paleomagnetic studies that suggest up to 90° of clockwise rotation of the western Transverse Ranges block that may have been driven large strike-slip fault movements, in contrast to the southern Coast Ranges block that has undergone little or no rotation (Fig. 2) (Hornafius et al., 1986). The SMB tectonic blocks are located in between rotating and non-rotating blocks and may have undergone a large amount of left lateral strike-slip movement (gray blocks in Fig. 2).

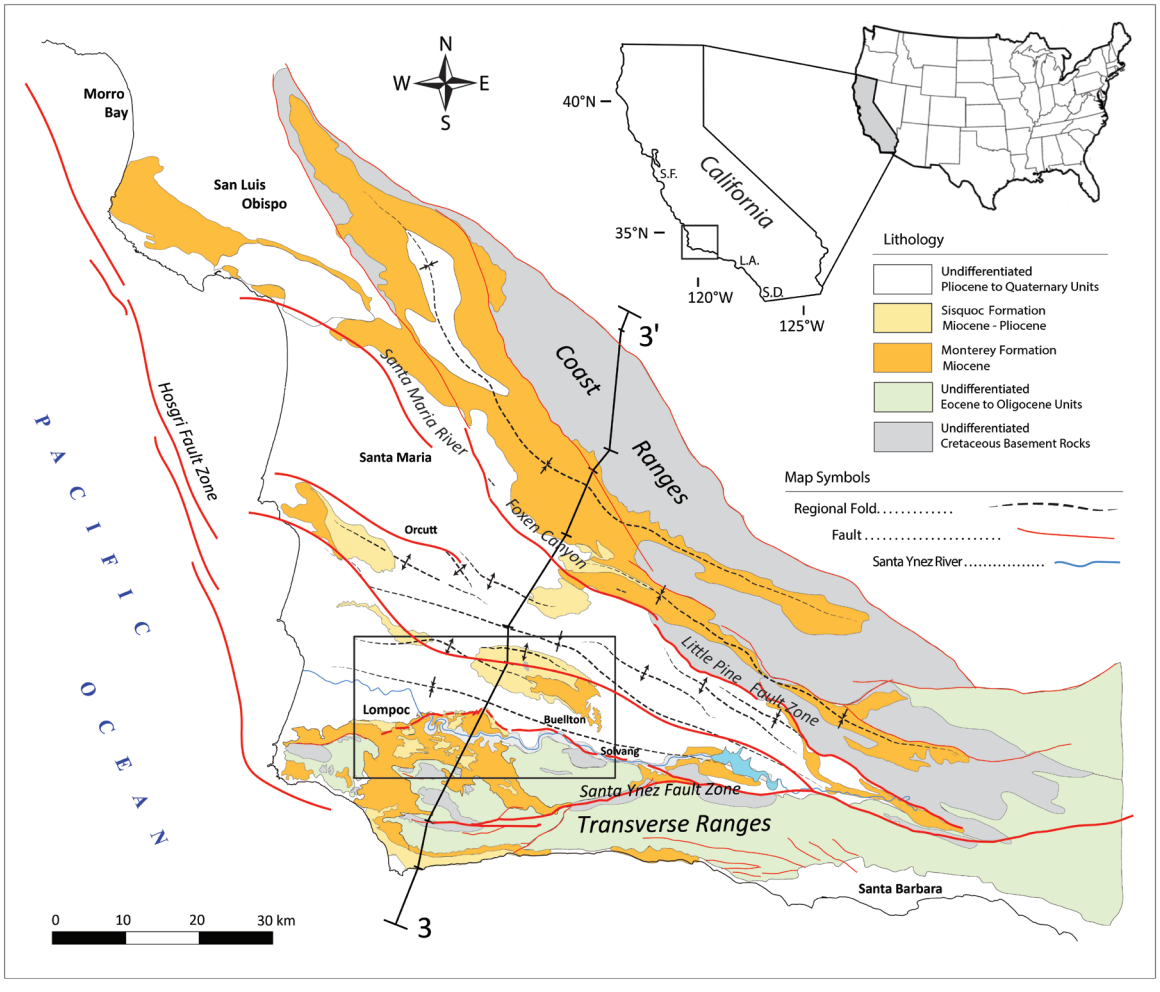

FIGURE 1. Regional geologic setting of the Santa Maria basin (SMB) area showing location of study area (black box). The SMB is located at the junction of the north-west trending Coast Ranges and the east-west trending Transverse Ranges. Structurally it is bounded by the Santa Maria River-, Foxen Canyon-, and Little Pine faults to the northeast, the Santa Ynez fault zone to the south, and the offshore Hosgri fault zone to the west. Basin internal structures are regional-scale faults and folds with westerly to northwesterly trends. The general stratigraphy is undifferentiated oceanic basement rocks of Jurassic and Cretaceous age, undifferentiated deep marine Eocene and nonmarine Oligocene units exposed along the basin boundaries, Miocene deep marine basin units of the Rincon, Tranquillon volcanics, Monterey and Sisquoc formations, and undifferentiated Pliocene to Quaternary shallow marine to terrestrial units.

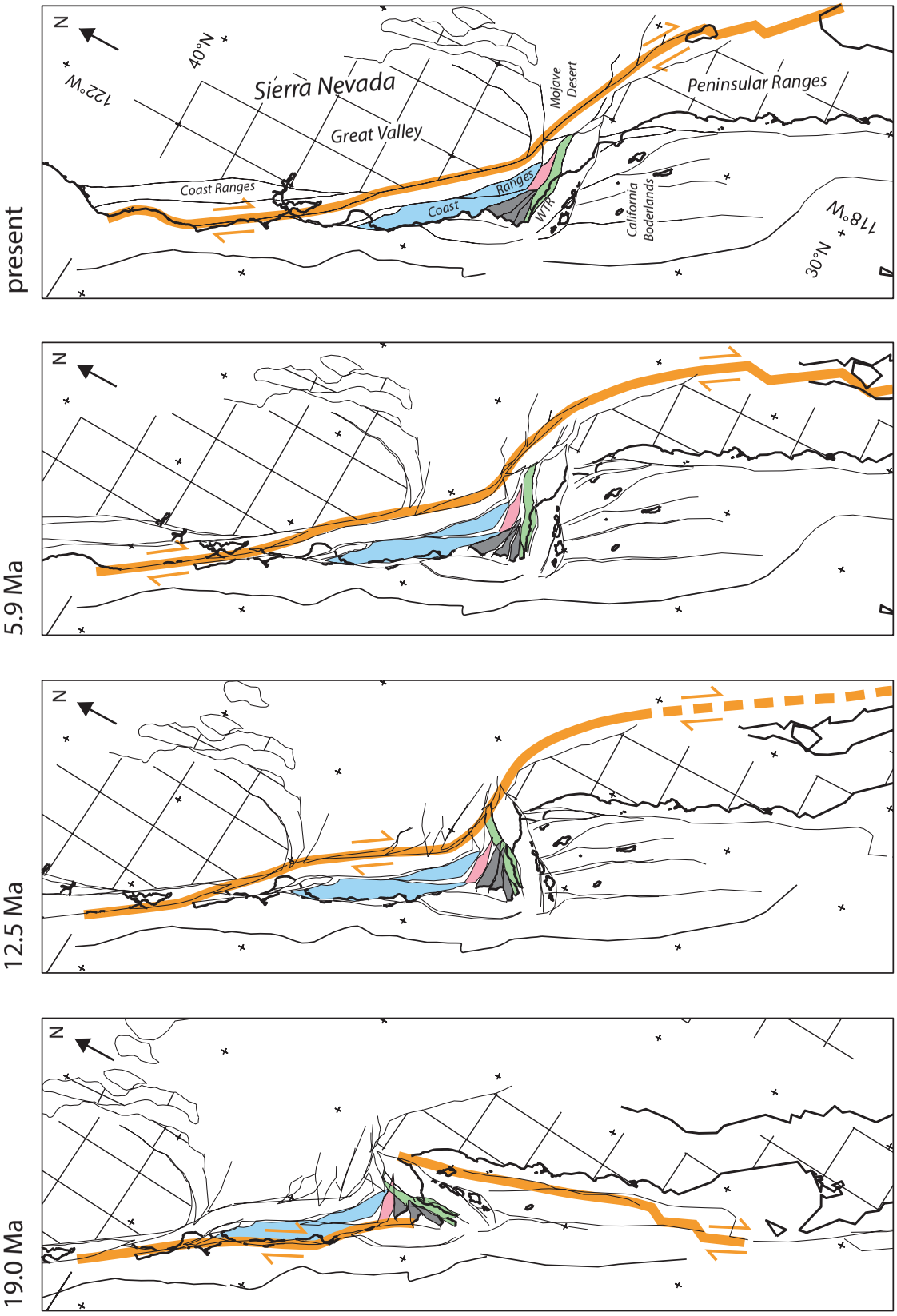
present
5.9 Ma
12.5 Ma
19.0 Ma
N
40°N
122°W
Sierra Nevada
Great Valley
Coast Ranges
Coast Ranges
WTR
Mojave Desert
Peninsular Ranges
California Boderlands
118°W
30°N

FIGURE 2. Interpretive kinematic reconstruction of southern and central California from 19 Ma to present based on paleomagnetic data. Thick black lines show the present day coastline, thin black lines show crustal blocks including the Santa Maria basin (SMB) blocks in grey, the Coast Ranges blocks in blue, the western Transverse Ranges (WTR) blocks in green, and the Mono-Sespe block in pink. Orange line highlights the fastest slipping fault trace in continental crust. The Sierra Nevada - Great Valley block and Peninsular Ranges block (denoted by grid pattern), are modeled as rigid crustal blocks. Note the kinematic behavior of the SMB crustal blocks (grey) forming a rift basin during transtension from 19 Ma to 5.9 Ma and uplift from 5.0 Ma to present during tanspression (modified after Wilson et al., 2005).

In the SMB, three tectonic models have been proposed for basin subsidence. The basin may have formed either as a pull-apart structure within a wrench system and large strike-slip offset (Hall, 1978), as a result of pure extension and clockwise rotation along a detachment above a metamorphic core complex (Crouch and Suppe, 1993), or as a result of local extension due to clockwise rotation of the Western Transverse Ranges and thermal subsidence (McCrory et al., 1995). Basin filling started with the primarily non-marine Lospe Formation that unconformably overlies Mesozoic basement, followed by the deep-marine Point Sal Formation. The greatest subsidence coincided with deposition of the siliceous, deep marine Monterey and Sisquoc Formations. Deposition of these sediments continued until the basin shallowed with the deposition of the Pliocene to Quaternary succession of Foxen Mudstone, Careaga Sandstone, and Paso Robles Formation.

Due to a change in the Pacific plate motion around 3 - 5 Ma (Engebretson and Cox, 1985), Miocene extension and rifting was followed by Pliocene to present shortening and uplift. Shortening is documented by extensive folds, thrust faults, angular unconformities, synorogenic deposits, and geodetic data (Reed and Hollister, 1936; Woodring and Bramlette, 1950; Hall, 1978; Dibblee, 1982; Namson and Davis, 1988b; Namson and Davis, 1990, Feigl et al., 1990). Four regional-scale anticlinal trends of 15-80 km in axial length and 2-3 km in structural relief dominate the surface geology throughout the SMB. These regional trends include the Lompoc-Purisima anticline, the Casmalia-Orcutt anticline, the Cat Canyon anticline, and the Point San Luis anticline (Fig. 1, 3). Regional-scale balanced cross-sections interpret the anticlinal trends to be fault-bend and fault propagation folds resulting from thrust ramps off thrust flats and a regional detachment at 11-14 km depths (Fig. 3) (Namson and Davis, 1990).

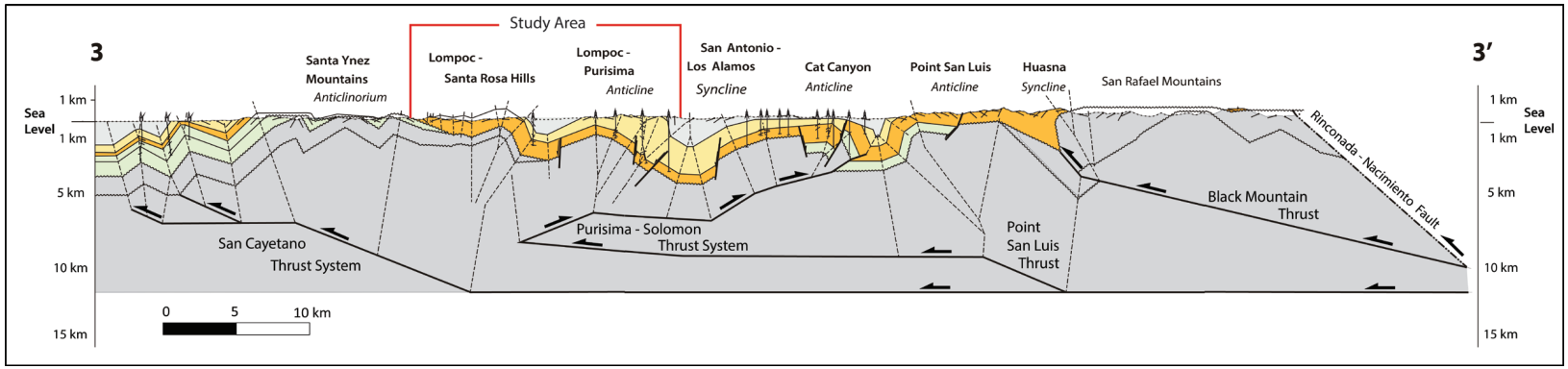

FIGURE 3. Regional balanced cross-section across the Santa Maria Basin. The cross section crosses four regional-scale anticlinal trends and interprets them to be caused by fault ramps above a regional detachment: The Lompoc-Purisima anticline, the Casmalia-Orcutt anticline, the Cat Canyon anticline, and the Point San Luis anticline (modified after Namson and Davis, 1990).

Two kinematic models have been proposed to explain Pliocene to present convergence and basin uplift. The first model suggests continued clockwise rotation of the western Transverse Ranges (Fig. 2) (Sorlien et al., 1999; McCrory et al., 2008). This model requires significant strike-slip offset at rotational boundaries and basin internal faults. A second model deals more directly with only Pliocene to present shortening (Namson and Davis, 1988a, 1988b, 1990) and earthquake focal mechanisms in coastal California (Zoback et al., 1987; Mount and Suppe, 1987) and invokes strain partitioning and requires little, or no rotation during the Pliocene and Quaternary (Fig. 4). In this model, transpression along the San Andreas active plate margin is resolved into two components: (1) pure strike slip along the San Andreas fault, and (2) north-south crustal shortening on either side of the fault (Namson and Davis, 1988b). Consequently, a number of large faults that originally served as extensional growth faults during the Miocene were subsequently inverted into thrust geometries (Namson and Davis, 1988b; Clark et al., 1991; Gutiérrez-Alonso and Gross, 1997).

The regional and most widespread contractional events in the SMB are recorded in two different episodes: The first one in the late Pliocene and a second one from the Pleistocene to present (Dibblee, 1950). The entire SMB area underwent a late Pliocene orogeny indicated by a widespread erosional unconformity at the base of the Careaga Sandstone. From late Pleistocene to present time the region underwent renewed deformation and uplift and attained the present topography during a second, ongoing uplift and erosional cycle (Dibblee, 1950). Localized uplift started earlier in the mid-Pliocene documented by thinning of the upper Sisquoc Formation onto growing topographic highs (Behl and Ingle, 1998), and possibly as early as latest Miocene to early Pliocene (McCrory et al., 1995).

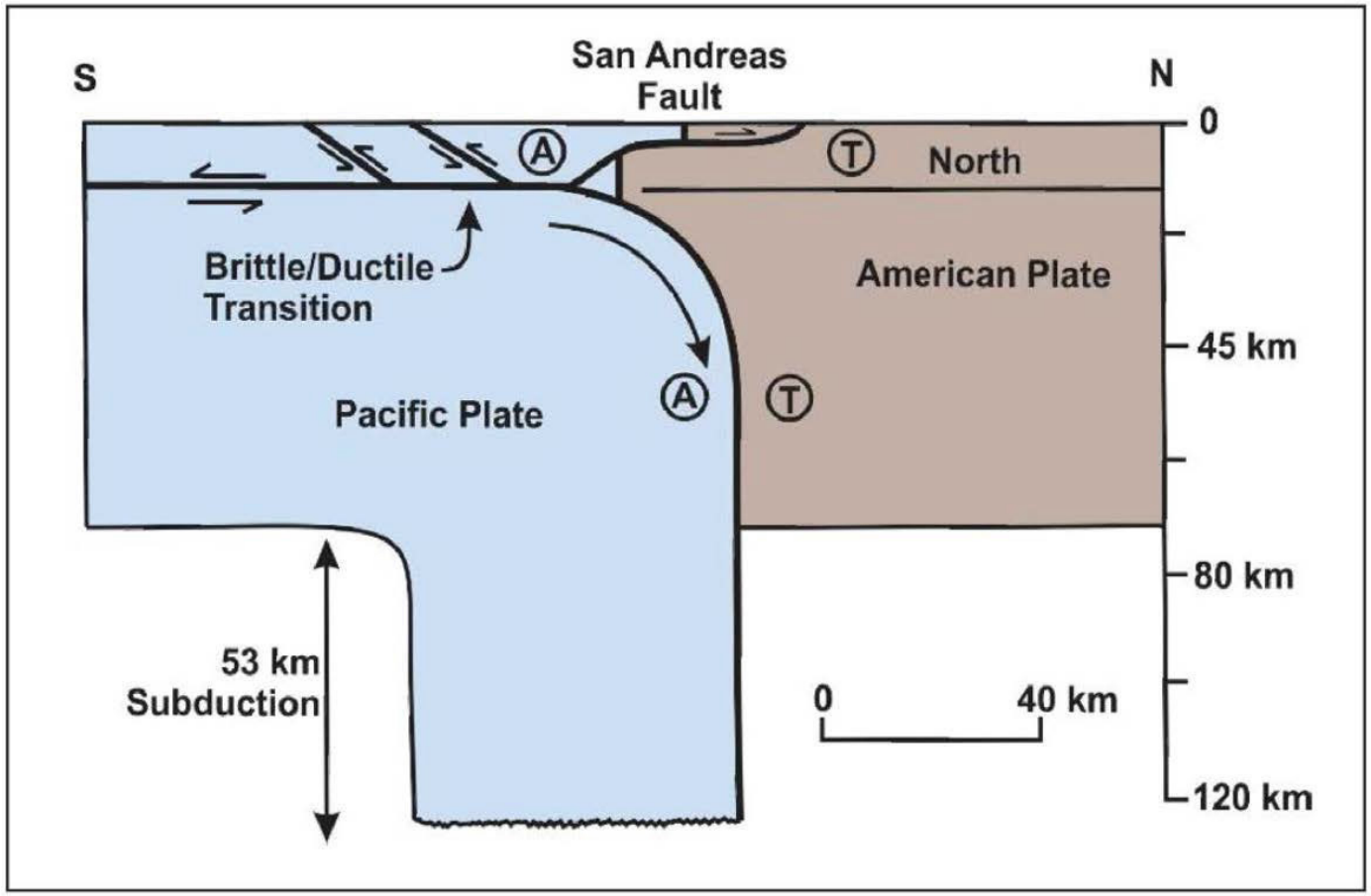

FIGURE 4. Strain partitioning model showing transpression along the San Andreas active plate margin is resolved into two components: (1) pure strike slip along the San Andreas fault, and (2) north-south crustal shortening on either side of the fault (modified after Namson and Davis, 1988).

Local Geology

The part of the southern SMB examined in this study exposes rocks of the Monterey and overlying Sisquoc formation over 340 km^2. Two study areas were chosen to investigate strain in the southern SMB (Fig. 5): 1) the Lompoc Hills, Santa Rosa Hills and Santa Rita Hills to the south, and 2) the Purisima Hills to the north. The southern study area is bounded by the Lompoc Valley and Santa Rita Valley to the north and the northern block of the Santa Ynez Mountains to the south. The northern study area is bounded by the Santa Rita Valley and Santa Ynez Valley to the south and the Los Alamos Valley to the north (Fig. 5). In the southern study area, the topography is controlled by three main drainages cutting through the Miocene rocks including the Santa Ynez River through the northeastern part, El Jaro Creek through the central part, and San Miguelito Canyon through the western part (Fig. 5). These drainages created excellent outcrops that allow structural mapping at outcrop-scale.

Map-Scale Structural Setting

In both study areas, the fold style diverges significantly from the regional fold belt of the SMB. The regional folds in the SMB have wavelengths of 5 to 10 km and axial lengths of up to 40 km (Fig. 1, 3). In contrast, the study areas are composed of localized east-west oriented folds with wavelengths ranging from 0.1 km to 3 km and axial lengths ranging from 0.5 km to 10 km (Fig. 6). These folds are almost entirely confined to the upper Monterey and Sisquoc formations and just a few structures with regional axial lengths of over 10 km extend into adjacent units of younger or older age outside of the study area. Only a few regional folds underlie the highly folded Monterey Formation. In the study areas, fold belts show different axial lengths (Fig. 6). In general, first order folds are above 10 km in axial length and are part of major structures that involve older and younger rocks. Second order folds are 0.5 - 8 km in axial length and represent

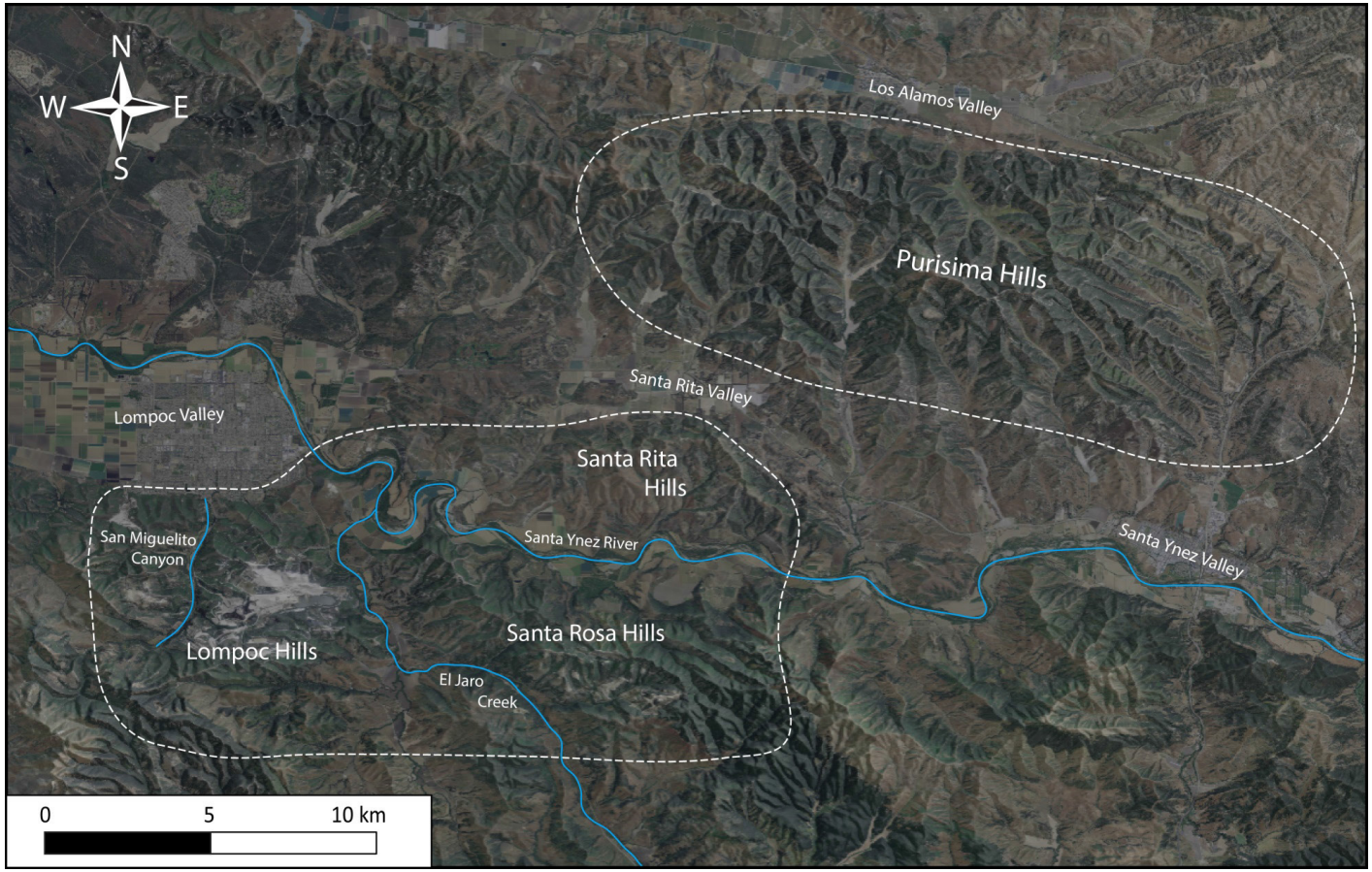

FIGURE 5. Physiographic setting and boundaries of study areas. White dashed lines showing boundaries of the two study areas.

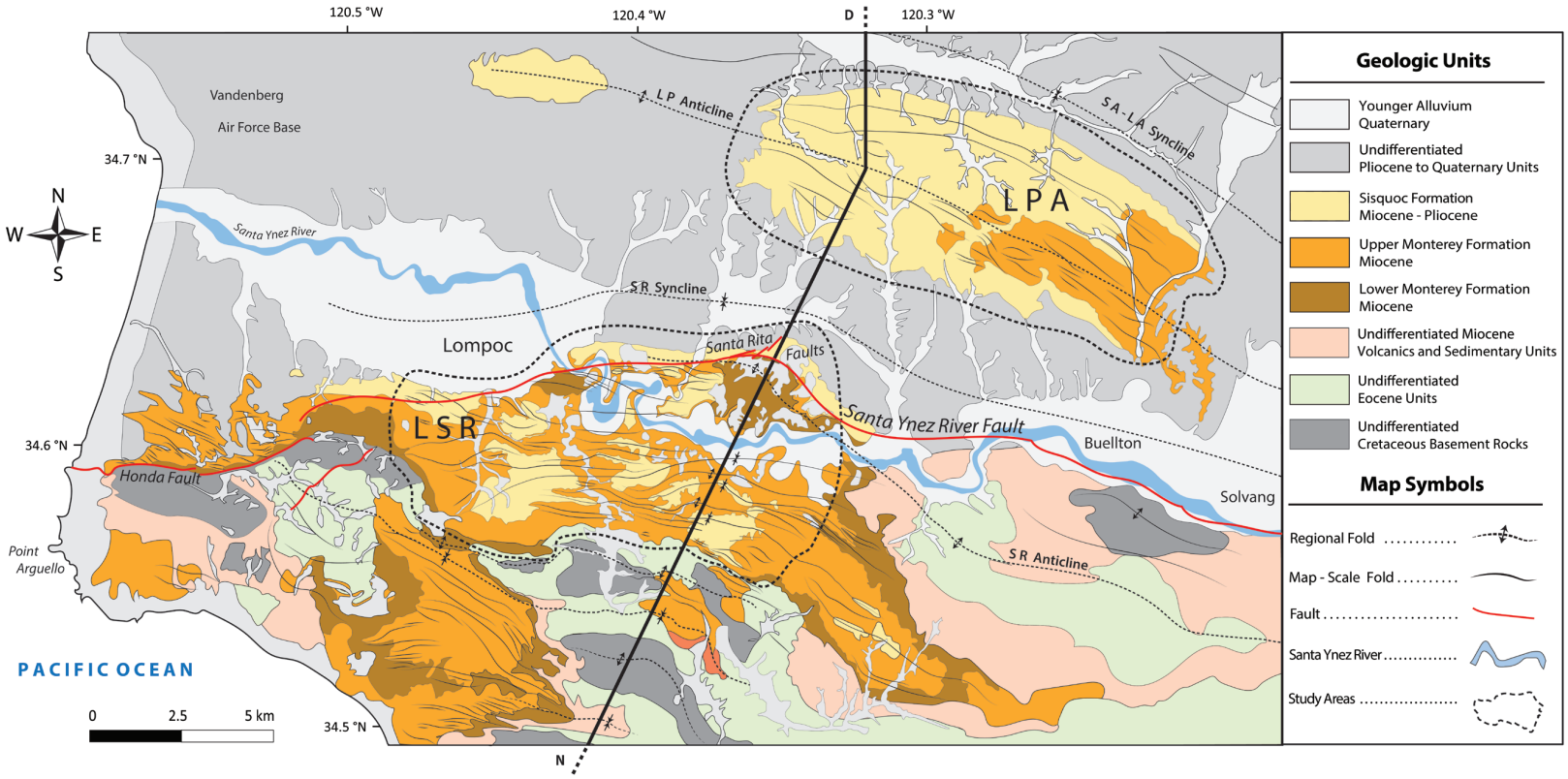

FIGURE 6. Geologic map (modified after Dibblee, 1950; and Dibblee and Ehrenspeck, 1988a, 1988b, 1988c, 1988d, 1988e, 1993a, 1993b) of the southern Santa Maria basin showing the two study areas: Lompoc-Purisima-Anticline (LPA) fold belt to the north, and the Lompoc-Santa Rosa (LSR) fold belt to the south (dashed polygons). Map displays the regional-scale fold belt , sub regional-scale folding in the Monterey and Sisquoc Formations, location of regional cross-section N-D (Namson and Davis, 1990).

the majority of folds. Third order folds are 0.1 - 0.5 km in axial length and occur in smaller sets (Fig. 6). Second and third order folds represent the majority of folds are confined to the upper Monterey and Sisquoc formations. Because of the spatial limitation of the folds to the described areas and the contrasting fold magnitude compared to the regional scale the two study areas will now be referred herein as the Lompoc - Santa Rosa fold belt (LSR) to the south and the Lompoc - Purisima Anticline fold belt (LPA) to the north (Fig. 6).

The LSR and LPA areas were mapped in detail by Dibblee (1950), and Dibblee and Ehrenspeck (1988a, 1988b, 1988c, 1988d, 1988e, 1993a, 1993b). The maps document a large amount of structural data, including bedding strike and dip, formation contacts, shape and orientation of synclinal and anticlinal fold axes, and faults (Fig. 6). In the LSR, the upper Monterey Formation is the dominant exposed formation. The Sisquoc Formation is only exposed within the major synclinal structures and to the north near where the LSR is buried underneath the Santa Rita Valley (Fig. 6). In the LSR, the aerial ratio of Sisquoc Formation to Monterey Formation exposure is about 1:4. In contrast, the Sisquoc Formation is the dominant exposed unit in the LPA with a Sisquoc Formation to Monterey Formation exposure ratio of 3:1 (Fig. 6).

Faults in the study area have been mapped by Dibblee (1950) and Hall (1982). Dibblee (1950) postulated that the intense folding south-west of the Santa Rita faults and north of the Honda fault are left-stepping en-echelon folds related in space and origin to left-lateral strike-slip movement (Fig. 6). Sylvester and Darrow (1979) used this observation as evidence for the existence of a major through-going strike-slip fault introduced as the Santa Ynez River fault. Hall (1982) mapped a through-going fault that he inferred as the Lompoc-Solvang fault from correlating contrasting basement rocks. Kinematic interpretations of fault movement propose the fault to be a left-lateral strike-slip fault (Dibblee, 1950; Sylvester and Darrow, 1979; Hornafius et

al., 1986; Sorlien et al., 1999). No work has been done that depicts the 2D or 3D subsurface geometry of the fault.

Outcrop-Scale Structural Setting

Rocks of the upper, thinly bedded siliceous member of the Monterey Formation in the LSR display intraformational deformation at outcrop-scale (Snyder, 1987; Gutiérrez-Alonso and Gross, 1997). This deformation includes a variety of different types of detachment folds and fault-propagation folds (Snyder, 1987) that are interpreted to be the result of blind thrusts splaying off detachment horizons at depth and bedding-plane detachments themselves folded progressively during deformation (Gutiérrez-Alonso and Gross, 1997). Folds at outcrop-scale are cylindrically shaped, nearly horizontal, and consistent with the regional fold axes and are, therefore inferred to be tectonic in origin (Gutiérrez-Alonso and Gross, 1997). The genesis of these Monterey Formation internal structures reflects a complex interplay of depositional, diagenetic, and tectonic events. Across the study area, domains with pervasive deformation are separated from areas of relatively unstrained strata at outcrop-scale. No work has been done that explains the reason for intensified outcrop-scale deformation in certain areas.

The Monterey and Sisquoc Formations

The Monterey and Sisquoc formations are geologic units well suited to quantify tectonic shortening and analyze structural and stratigraphic influences because (1) they were deposited during the Miocene to early Pliocene prior to the widespread regional contraction, (2) their largely distinct diagenetic state provides quantifiable structures reflecting different rock mechanics at map-scale and outcrop-scale, and (3) they are laterally well exposed over a 340 km^2 area in the study areas.

The Monterey and Sisquoc formations have accommodated tectonic shortening with contrasting deformational styles in different locations and stratigraphic intervals (Snyder et al., 1983; Snyder, 1987; Gutiérrez-Alonso and Gross, 1997). Even within a single outcrop, and therefore identical tectonic conditions, beds can provide widely different structures and individual styles of tectonic deformation. This is due to a complicated interplay between the deformational and the diagenetic history of the bedded siliceous sedimentary rocks that affects their deformational style (Snyder et al., 1983; Snyder, 1987; Behl, 1992).

The Monterey and overlying Sisquoc Formations in the study area preserve siliceous sediments in a complete spectrum of diagenetic stages. The degree of the diagenetic stage is controlled by the initial sediment composition and temperature with depth (Fig. 7). This enables dramatic variations in lithologies even within a single outcrop from opal-A (diatomaceous sediments composed of X-ray amorphous silica) to opal-CT (metastable silica composed of poorly ordered, hydrous cristobalite and tridymite) to quartz bearing rocks (Isaacs, 1981). With changes in silica phase, porosity can change from about 80% in opal-A phase rocks to almost 0% in quartz phase rocks (Fig. 7) (Isaacs, 1981). Depending on the ratio of detritus vs. silica of a stratigraphic interval, the different lithologies can occur in stratigraphic packages of alternating orders and thickness (Fig. 8). In general, the lithologies in the stratigraphically higher Sisquoc Formation are all composed of opal-A phase diatomaceous sediments with alternating detritus content (Fig. 8). In contrast, the lithologies in the underlying upper Monterey Formation are highly heterogeneous and progressively composed of more opal-CT phase rocks of higher competence down-section (Fig. 8). For simplicity, all porous opal-A diatomaceous rocks will be termed as diatomite, and all hard to brittle opal-CT diagenetic rocks will be termed as chert/porcelanite, regardless of variations in their detritus content.

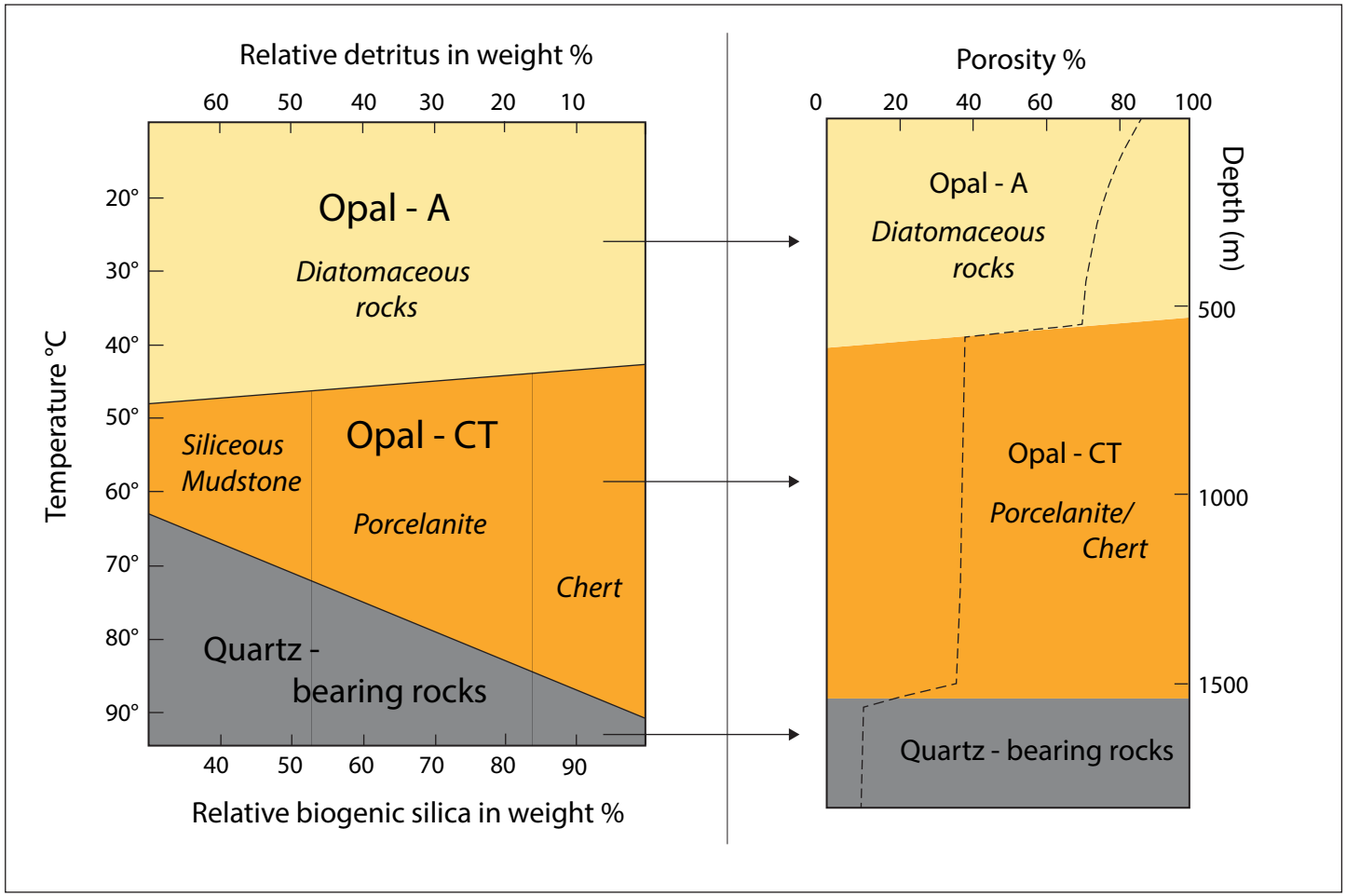

FIGURE 7. Silica phase changes during diagenesis and associated lithologies (left) (modified after Isaacs, 1981 and Behl, 1992) and stepped changes in porosity with depth (right) (modified after Isaacs, 1981).

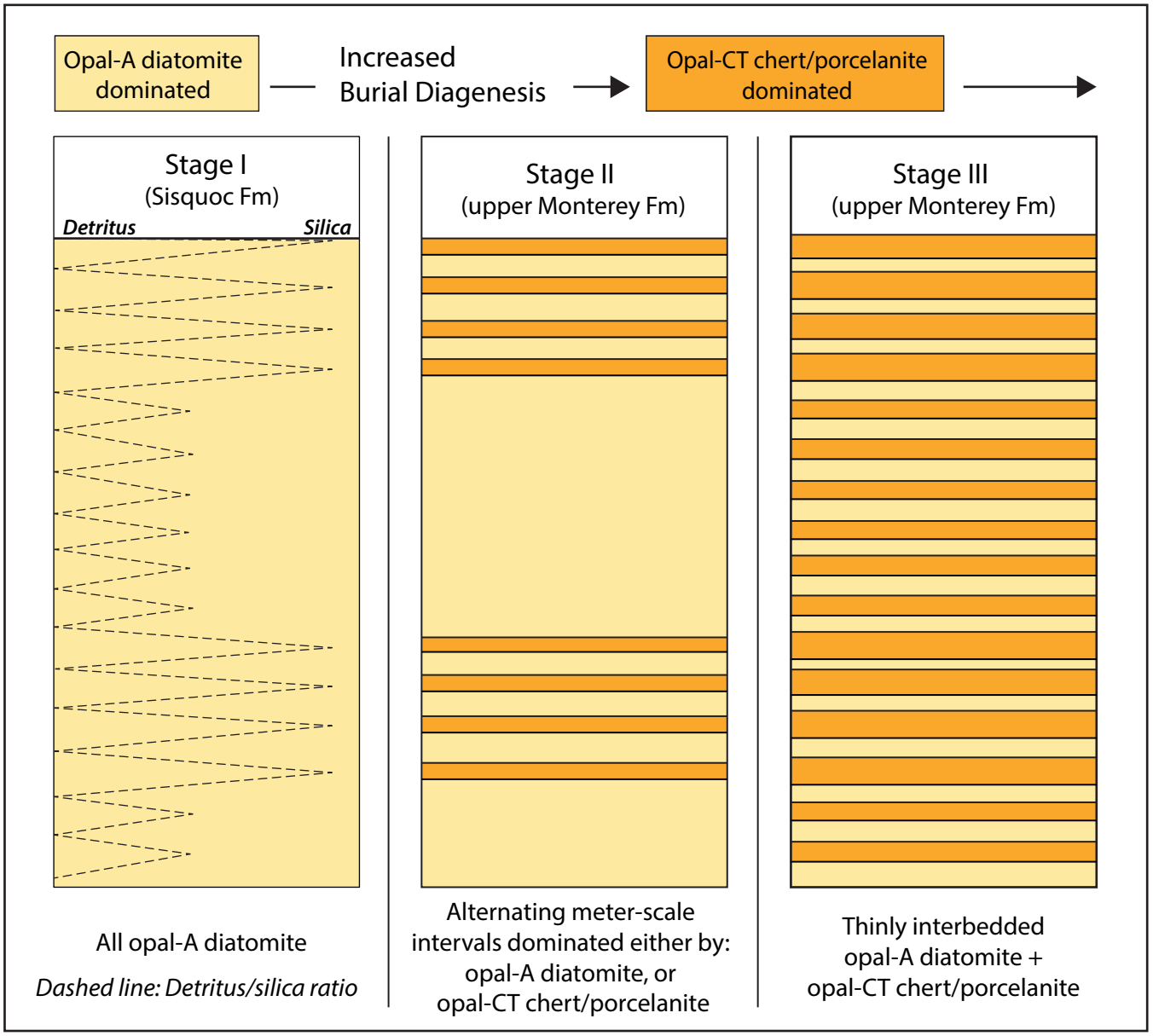
Opal-A diatomite dominated
Increased Burial Diagenesis
Opal-CT chert/porcelanite dominated
Stage I
(Sisquoc Fm)
Detritus
Silica
Stage II
(upper Monterey Fm)
Stage III
(upper Monterey Fm)
All opal-A diatomite
Dashed line: Detritus/silica ratio
Alternating meter-scale intervals dominated either by: opal-A diatomite, or opal-CT chert/porcelanite
Thinly interbedded opal-A diatomite + opal-CT chert/porcelanite

FIGURE 8. Sketch of diagenetic modification of a representative section in the upper Monterey Formation. Note that the primary composition (silica/detritus ratio) of the sediments shown in stage 1 controls the kinetics of silica phase transitions shown in stage II and stage III. Beds containing high amounts of silica undergo diagenetic modification early in burial and beds containing high amounts of detritus might not undergo diagenesis until later stages. This opens the possibility of heterogeneous rock packages of alternating lithologies between porous diatomite and competent chert/porcelanite. The three stages coexist in the study area with the Sisquoc Formation that is representative for stage I, and the upper Monterey Formation that is representative for stage II and stage III.

Variations in physical properties of these rocks that influence their distinct structural behavior as a result of initial sediment composition and diagenetic modification have been described as mechanical stratigraphy (Gross et al., 1997). In general, mechanical stratigraphy is defined as the subdivision of a rock section into discrete units by their deformational style, structures, or mechanical properties (Laubach et al., 2009). In the study areas, the upper Monterey Formation is largely composed of thinly bedded intervals of incompetent, porous diatomite (about 40 - 60 %) and competent hard to brittle chert/porcelanite (about 40 - 60%). Bed thicknesses typically range from 5 - 20 cm (with the full range spanning from <1 cm to ~1 m) resulting in a heterogeneous rock mass where style of deformation is a function of mechanical stratigraphy (Gross et al., 1997). The overlying Sisquoc Formation is less diagenetically altered and composed of thick bedded, highly porous diatomite (Fig. 8).

In short, depositional, diagenetic, and tectonic events combine to form a variety of deformational styles among different lithologies and mechanical units. The great mechanical anisotropy between the Sisquoc and the upper Monterey Formation provide the basis for development of different deformational mechanisms in close proximity, including both consumption of strain via volume reduction in diatomites (pure shear) and complex interplay of flexural-slip, folding and faulting within interbedded diatomite and chert/porcelanite (simple shear).

CHAPTER 3

MAP-SCALE FOLD STRAIN ANALYSIS

Limitations and Assumptions

Inherent in all strain analysis studies are the problems of heterogeneity due to the partitioning of strain. Depending on locality, tectonic strain can be of different configuration and degree. This study is a two-dimensional approach based on construction of cross-sections that measure the projected line-lengths of the upper Monterey Formation and the overlying Sisquoc Formation. The construction of these sections assumes no movement along strike of the bedding because movement perpendicular to the direction of fold strain is significantly small relative to movement parallel to it. The main data set for the construction of the cross-sections is derived from geologic maps (Dibblee, 1950; Dibblee and Ehrenspeck 1988a, 1988b, 1988c, 1988d, 1988e, 1993a, 1993b). These maps show that fold structures are highly heterogeneous and have significant differences in fold orientations and axial lengths. There are areas of intense deformation displayed by smaller wavelengths, whereas other areas display much broader wavelengths (Fig. 6). Strike and dip orientations of bedding fluctuate significantly along the flanks of anticlinal or synclinal fold axes and throughout the LSR and LPA, making even a single structure along strike extremely heterogeneous with multiple possibilities of how to construct fold geometries and document the orientation and length of folds. Dense vegetation in the eastern part of the study area of the LSR and throughout the LPA possibly hides important structural data, which might contribute to more strain information in the Monterey and Sisquoc rocks at map-scale and outcrop-scale. Therefore, strain analysis in this study assumes a minimum in tectonic shortening.

Purpose and Selection of Study Area

Tectonic shortening was quantified in the upper Monterey and Sisquoc formations in order to (1) address the impact of lithology on deformational behavior, (2) better depict variation of strain intensity with space and scale, and (3) examine if more detailed fold strain analyses in fold-and-thrust belts can lead to revised interpretations of thrust emplacement. Nineteen line-length-sections across the LSR, and nine line-length-sections across the LPA were constructed to generate the key data set for shortening estimates and fold geometry description through the uniformly diatomaceous and thick-bedded Sisquoc Formation of low competence (diatomite), and the heterogeneous and thinly interbedded upper Monterey Formation of higher competence (diatomite and chert/porcelanite) (Fig. 9). Although the LSR and the LPA study areas are relatively close to each other, results were plotted separately in order to avoid possible problems of regional strain heterogeneity that might affect the local strain regime. A basement involved balanced cross-section was constructed in order to show how the results found in this study can affect regional geometric models of fold and thrust belts. This has been achieved by linking deformation of the Monterey and Sisquoc formations with deeper subsurface structures via a tectonic wedge model.

Methods

Line-length-sections and a balanced cross-section were constructed using LithoTect structural modelling software. The data set used for surface and subsurface modeling included over 600 strikes and dips from geologic maps at a scale of 1:24,000 (Dibblee, 1950, 1988 a-e, 1993 a,b) with an additional 100 strikes and dips from field mapping during this study, pre-Monterey Formation subcrop and structure contour maps at a scale of 1:62,500 (Hall, 1982), eleven exploration wells, and 10 meter resolution digital elevation models. Line-length-sections

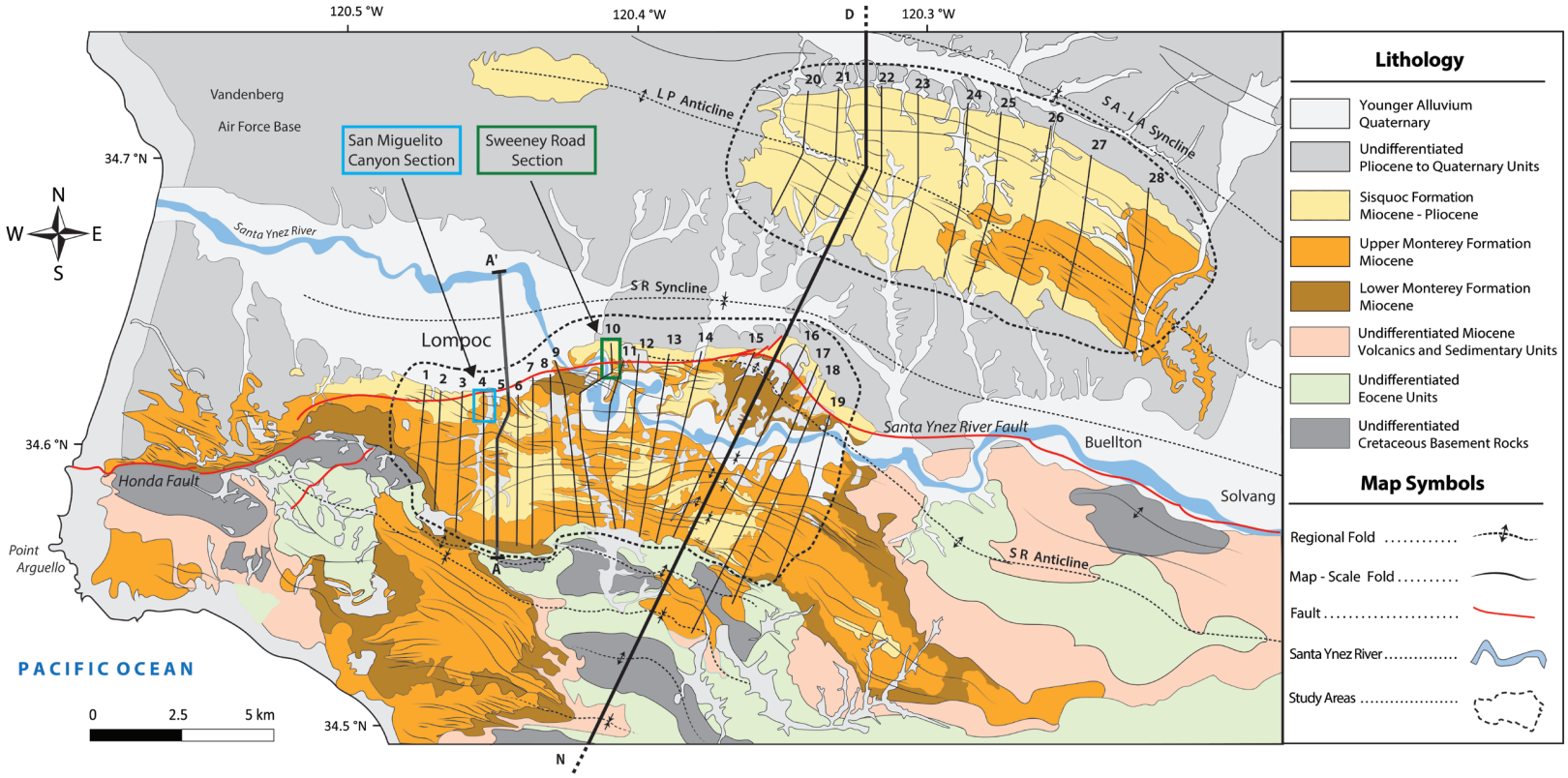

FIGURE 9. Locations of line-length-sections created in this study, and location of outcrop-scale structural analysis at Sweeney Road (green box at line-length-section 10) and San Miguelito Canyon (blue box at line-length-section 4).

were constructed with a five-step procedure: First, geologic maps, well data, and digital elevation models were loaded into a LithoTect project. Structural surface data including strike and dip orientation, formation contacts, and wells were digitized. Second, nineteen transects in the LSR and nine transects in the LPA were chosen parallel to principal convergent strain direction that is perpendicular to the major fold axes (Fig. 9). The average distance between each transect is 0.7 km for the LSR and 1.0 km for the LPA, providing high resolution strain data along fold strike. Third, surface digital elevation models and formation contacts were extracted to 2-dimensional section profiles. Fourth, dip data and well data were projected along fold strike to perform overall structural modeling normal to strike. Dip projection was always < 200 m, and well projection was always < 400 m. In a fifth step, line-length balancing was performed by creating dip domains with kink-geometries similar to the cross-section construction by Namson and Davis (1990) (Fig. 10). Total shortening for each line-length-section was quantified by subtracting the profile-length from the line-length of each section.

For each profile:

$$\text{Total Shortening [km]} = l_0\ \text{[km]} - l_1\ \text{[km]}$$

and,

$$\text{Total Shortening [\%]} = \frac{l_0\ \text{[km]} - l_1\ \text{[km]}}{l_0\ \text{[km]}}$$

where l_0 is the section line-length, and l_1 is the profile-length (Fig. 11).

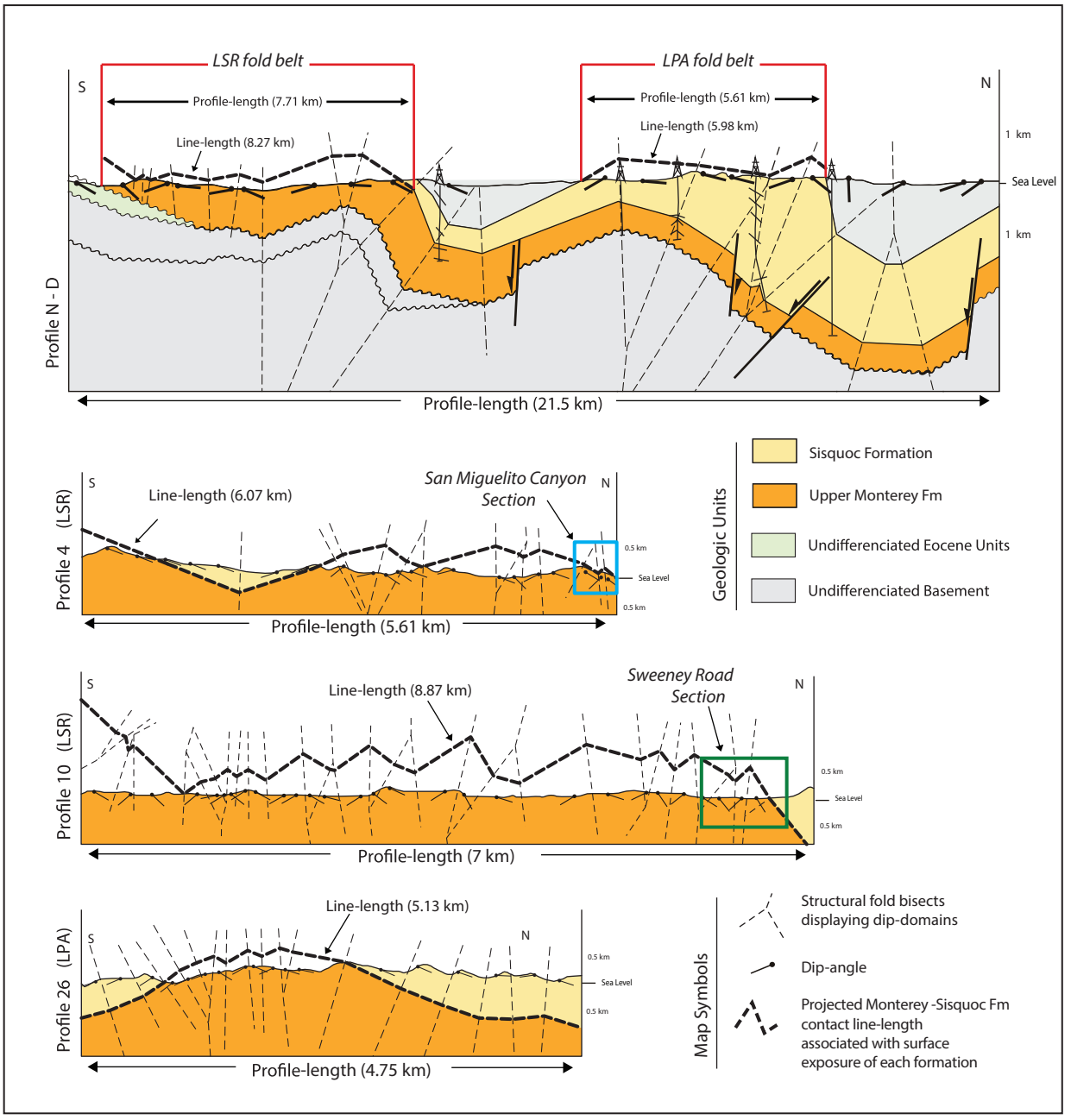

FIGURE 10. Construction method of line-length sections. Top section showing the portion of cross-section 3-3' by Namson and Davis (1990). Lower three sections show construction method of line-length sections. Profiles 4, 10, and 14 are representative sections from the LSR and LPA created in this study

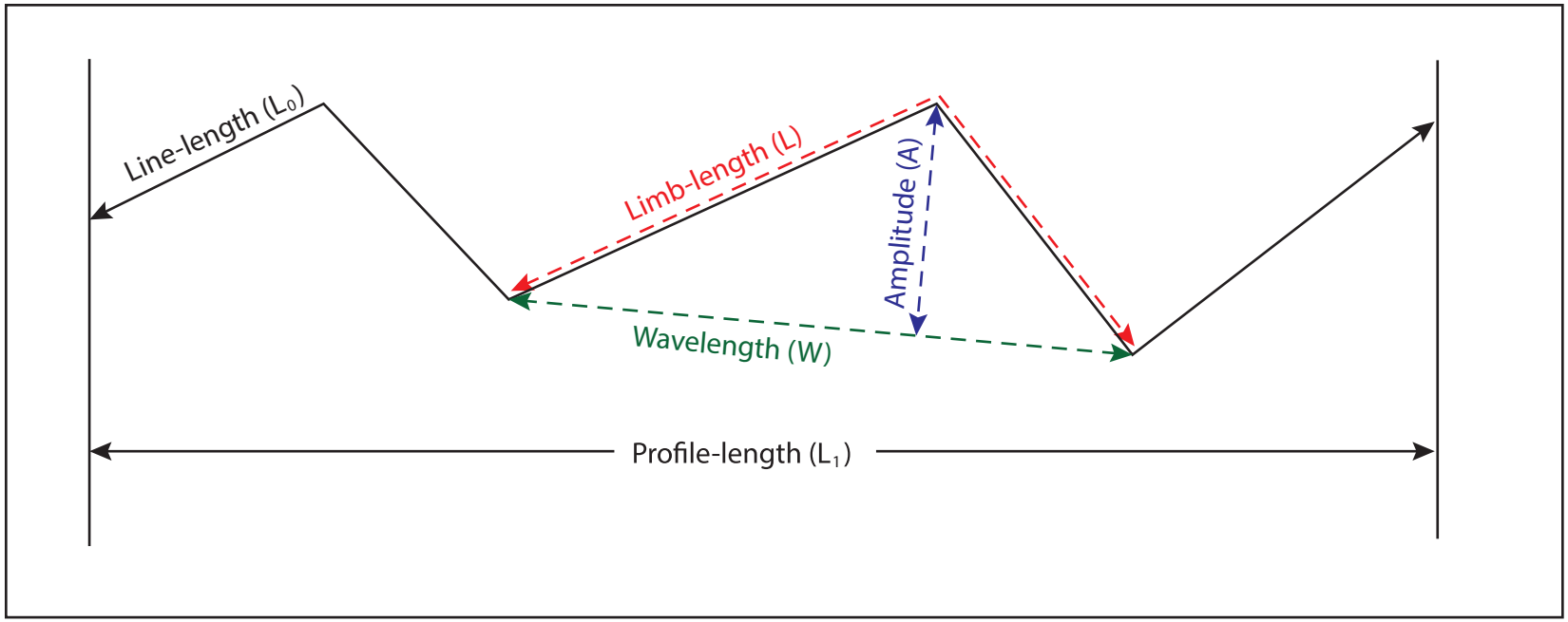

FIGURE 11. Schematic line-length-section showing different section components used for shortening calculations and fold geometry analyses.

In order to test the influence of lithology on the observable strain magnitude, line-lengths were compared between the sections that transect the porous, massive-bedded Sisquoc Formation and sections that transect the less porous, thin-bedded upper Monterey Formation. In the LSR and LPA, nine sections transect surface exposure of only Monterey Formation or Sisquoc Formation (Fig. 9). However, nineteen sections transect exposure of both the Monterey Formation and the Sisquoc Formation (Fig. 9). These sections were constructed using structural surface data from both units. The full line-length-section in these profiles are a mixture, with segments that represent strain in the Monterey Formation and segments that represent strain in the Sisquoc Formation, respectively. Therefore, the profiles measure strain along the projected Monterey and Sisquoc contact and are not representative for a single unit (Fig. 10). In the sections constructed using data from both formations, line-length segments of the Monterey Formation and the Sisquoc Formation were quantified separately in order to derive the total profile length and shortening values for the Monterey Formation and Sisquoc Formation. This allowed separately measuring the contribution of both units to the total amount of shortening. For sections with heterogeneous lithology the shortening along the line-length-section is calculated as:

$$\text{Shortening}_{\text{Monterey}}\,[\%] = \frac{\Sigma\, l_{0\,\text{Monterey}}\,[\text{km}] - \Sigma\, l_{1\,\text{Monterey}}\,[\text{km}]}{\Sigma\, l_{0\,\text{Monterey}}\,[\text{km}]} \times 100$$

and,

$$\text{Shortening}_{\text{Sisquoc}}\,[\%] = \frac{\Sigma\, l_{0\,\text{Sisquoc}}\,[\text{km}] - \Sigma\, l_{1\,\text{Sisquoc}}\,[\text{km}]}{\Sigma\, l_{0\,\text{Sisquoc}}\,[\text{km}]} \times 100$$

where Σl_0 Monterey and Σl_0 Sisquoc is the sum of the Monterey-Sisquoc formational contact line-lengths associated with surface exposure of either formation, and Σl_1 Monterey and Σl_1 Sisquoc the sum of the profile length of each unit, respectively. The contribution of shortening in the Sisquoc Formation and shortening in the Monterey Formation to the total shortening of each heterogeneous lithology line-length-section is shown by the shortening ratio "Shortening $_{\text{Sisquoc}}$: Shortening $_{\text{Monterey}}$" (Table 1).

In order to better understand the differences in degree of shortening between the Monterey and Sisquoc Formations, fold geometry analysis was performed for each line-length-section in the LSR and LPA. In general, each section shows unequal fold limb lengths across fold axes and usually one limb dips more steeply than the other resulting in asymmetrical and non-periodical fold geometries (Fig. 10). First, fold interlimb angles were measured for each fold. Folds in the Sisquoc and Monterey Formations were classified after Ramsay (1974) between gentle, open, and close fold angles. Second, fold wavelengths were measured as the distance between two successive anticlinal, or synclinal hinges (Fig. 11). Because of the asymmetric and non-periodical fold geometries, the amplitudes could not be measured along the axial plane from a median surface to the hinges as suggested by Frehner (2016). Instead, amplitudes were measured by creating the orthogonal between the hinge and the wavelength line for each fold (Fig. 11). Third, differences in degree of shortening between the Sisquoc Formation and the Monterey Formation have been quantified by plotting fold amplitude to fold shortening ratios for each fold in the LSR and LPA. Amplitudes were measured as just described. Fold shortening (FS) has been calculated for each fold using the wavelength (W) and the limb-length (L) of synclines and anticlines (Fig. 11). For each fold:

$$FS\ [km] = L\ [km] - W\ [km].$$

TABLE 1. Map-Scale Strain Analysis Results

	Total Profile Shortening				Sisquoc Formation					Monterey Formation					Tsq : Tm
LSR	Profile-Length [km]	Line-Length [km]	Shortening [km]	Shortening [%]	Profile - Length [km]	[%]	Line-Length [km]	Shortening [km]	Shortening [%]	Profile - Length [km]	[%]	Line-Length [km]	Shortening [km]	Shortening [%]	Shortening
1	3.57	4.02	0.46	11.32	0.93	26.11	1.11	0.18	15.90	2.63	73.89	2.91	0.28	9.61	1.65:1
2	4.41	5.22	0.81	15.55	1.18	26.88	1.56	0.38	24.20	3.22	73.12	3.65	0.43	11.85	2.04:1
3	5.41	5.95	0.54	9.13	1.10	20.28	1.25	0.16	12.53	4.31	79.72	4.70	0.39	8.24	1.52:1
4	5.61	6.07	0.46	7.58	1.48	26.38	1.57	0.09	5.73	4.14	73.62	4.50	0.36	8.00	0.72:1
5	6.45	7.42	0.97	13.01	2.75	42.58	2.92	0.17	5.89	3.71	57.42	4.50	0.79	17.63	0.33:1
6	5.76	6.09	0.34	5.51	4.16	72.18	4.33	0.17	3.91	1.60	27.82	1.77	0.17	9.49	0.41:1
7	6.60	7.11	0.51	7.13	3.59	54.39	3.78	0.19	5.03	3.01	45.61	3.33	0.32	9.69	0.52:1
8	6.03	6.68	0.65	9.73	2.06	34.16	2.19	0.13	5.94	3.97	65.84	4.49	0.52	11.58	0.51:1
9	6.39	7.32	0.93	12.69	0	0	0	0		6.39	100	7.32	0.93	12.69	
10	7.00	8.87	1.87	21.08	0	0	0	0		7.00	100	8.87	1.87	21.12	
11	6.25	7.40	1.16	15.61	0	0	0	0		6.25	100	7.40	1.16	15.61	
12	6.28	7.55	1.27	16.77	2.28	36.30	2.59	0.31	11.87	4.00	63.70	4.92	0.92	18.70	0.63:1
13	6.78	7.60	0.82	10.79	2.83	41.74	3.20	0.37	11.56	3.95	58.26	4.40	0.45	10.23	1.13:1
14	8.44	9.18	0.74	8.06	2.89	34.24	3.00	0.11	3.67	5.55	65.76	6.17	0.62	10.05	0.36:1
15	7.76	8.55	0.79	9.24	1.04	13.40	1.13	0.09	7.96	6.72	86.60	7.41	0.69	9.31	0.86:1
ND	7.71	8.27	0.56	6.77											
16	8.60	9.21	0.61	6.66	2.10	24.42	2.21	0.11	4.76	6.50	75.58	7.01	0.51	7.26	0.66:1
17	11.51	13.21	1.69	12.82	3.13	27.19	3.50	0.37	10.57	8.38	72.81	9.71	1.32	13.62	0.78:1
18	9.34	10.55	1.21	11.44	1.53	16.42	1.63	0.10	6.06	7.81	83.58	8.92	1.11	12.43	0.49:1
19	7.48	9.09	1.61	17.72	0.72	0	0.77	0.05	6.14	6.76	100	8.32	1.56	18.79	0.33:1
Mean				11.43					6.36					12.13	0.52:1
LPA	Profile-Length [km]	Line-Length [km]	Shortening [km]	Shortening [%]	Profile - Length [km]	[%]	Line-Length [km]	Shortening [km]	Shortening [%]	Profile - Length [km]	[%]	Line-Length [km]	Shortening [km]	Shortening [%]	Tsq : Tm Short.
20	4.08	4.30	0.22	5.19	4.08	100	4.30	0.22	5.19	0	0	0	0		
21	5.41	5.68	0.27	4.67	5.41	100	5.68	0.27	4.67	0	0	0	0		
ND	5.61	5.98	0.37	6.19											
22	5.68	6.07	0.39	6.38	5.68	100	6.07	0.39	6.38	0	0	0	0		
23	6.37	6.79	0.41	6.10	6.37	100	6.79	0.41	6.10	0	0	0	0		
24	5.83	6.14	0.31	5.04	4.72	80.97	4.94	0.22	4.53	1.11	19.03	1.19	0.08	7.04	0.64:1
25	5.76	6.58	0.82	12.45	4.43	76.91	5.04	0.61	12.18	1.34	23.09	1.53	0.20	12.78	0.95:1
26	4.75	5.13	0.38	7.35	2.58	54.28	2.77	0.19	6.86	2.17	45.72	2.35	0.17	7.33	0.94:1
27	4.62	5.34	0.72	13.44	2.07	44.69	2.14	0.08	3.55	2.56	55.31	3.20	0.64	20.07	0.18:1
28	4.59	5.52	0.93	16.77	0	0	0	0		4.59	100	5.52	0.93	16.77	
Mean				8.36					6.18					12.80	0.48:1

Results

The data show significant strain variation along strike of the fold axes over short distances (Fig. 12). In the LSR, shortening values range from 5.5 % (profile 6) to 21.1 % (profile 10). From the western to the eastern part of the LSR, areas of high strain are separated by areas of low strain. In general, three high-strain areas occur in the most western, in the central, and the most eastern part (Fig. 13). Between these areas of higher strain, shortening significantly decreases over distances of just a few kilometers. In the LPA, shortening values range from 4.7 % (profile 21) to 16.8 % (profile 28). The magnitude of shortening is distinctly lower in the western part and higher in the eastern part. Significant increase in strain occurs, like in the LSR, over just a few kilometers of along-strike extent (Fig. 12). The contribution of shortening in the Sisquoc Formation and shortening in the Monterey Formation to the total shortening shows a mean ratio of 0.52 : 1 in the LSR and 0.48 : 1 in the LPA between shortening expressed in the Sisquoc Formation vs. Monterey Formation shortening (Table 1).

In order to illustrate strain variation between the Monterey Formation and Sisquoc Formation, total shortening for each line-length-section was plotted over the percentage of Sisquoc and Monterey Formation profile length to the total profile length for each line-length-section (Fig. 13). In both study areas, results show a negative trend between the amount of shortening and the amount of Sisquoc Formation exposure, and a positive trend between the amount of total shortening and the amount of Monterey Formation exposure to the total profile length, respectively. In other words, low shortening rates are observed in sections with high exposure of Sisquoc Formation, and high shortening rates are observed in sections with few exposure of Sisquoc Formation. Transects with mostly Monterey exposures show the highest

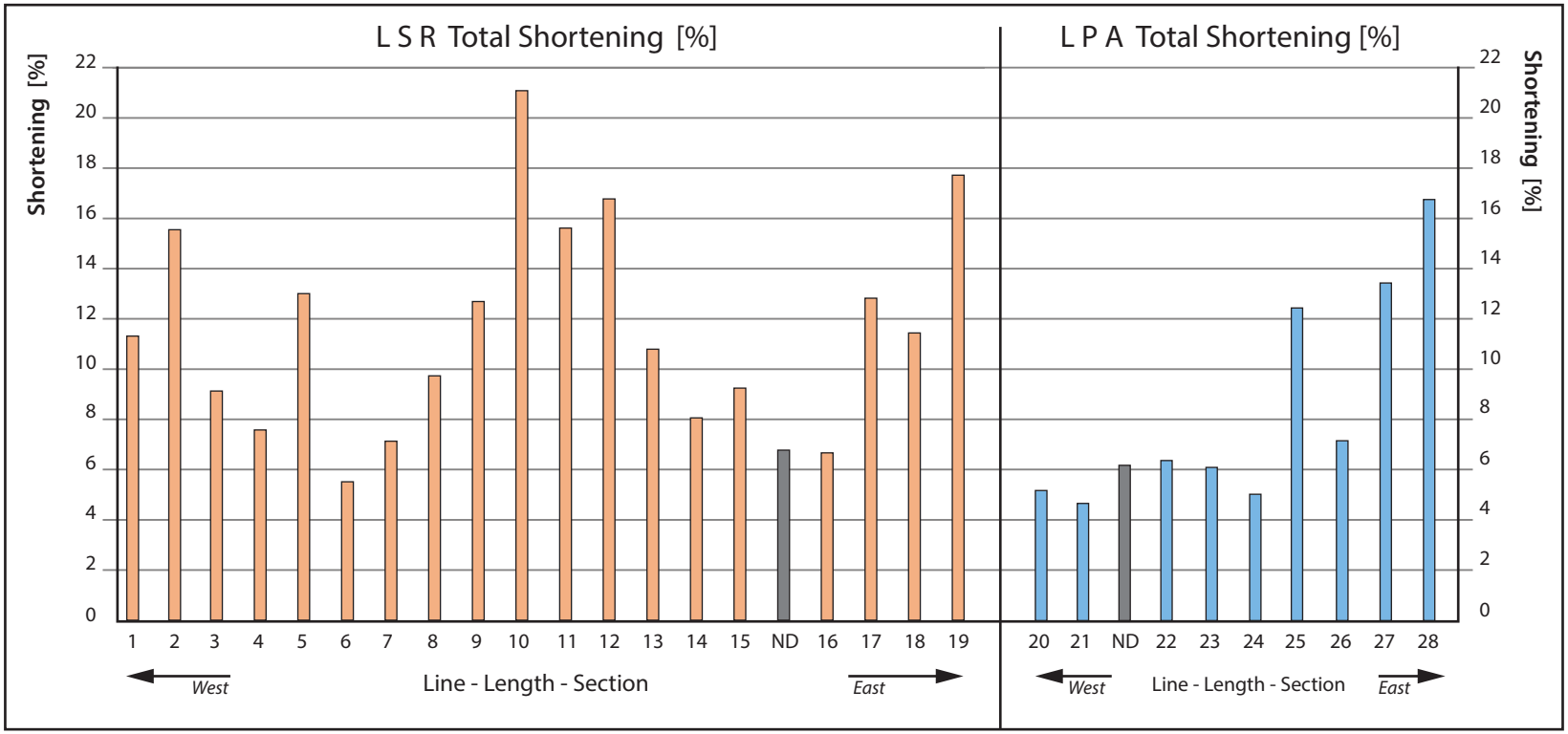

FIGURE 12. Histogram of shortening estimates in the LSR (orange) and LPA (blue). Line-length estimates across the LSR and LPA by Namson and Davis (1990) are shown in grey.

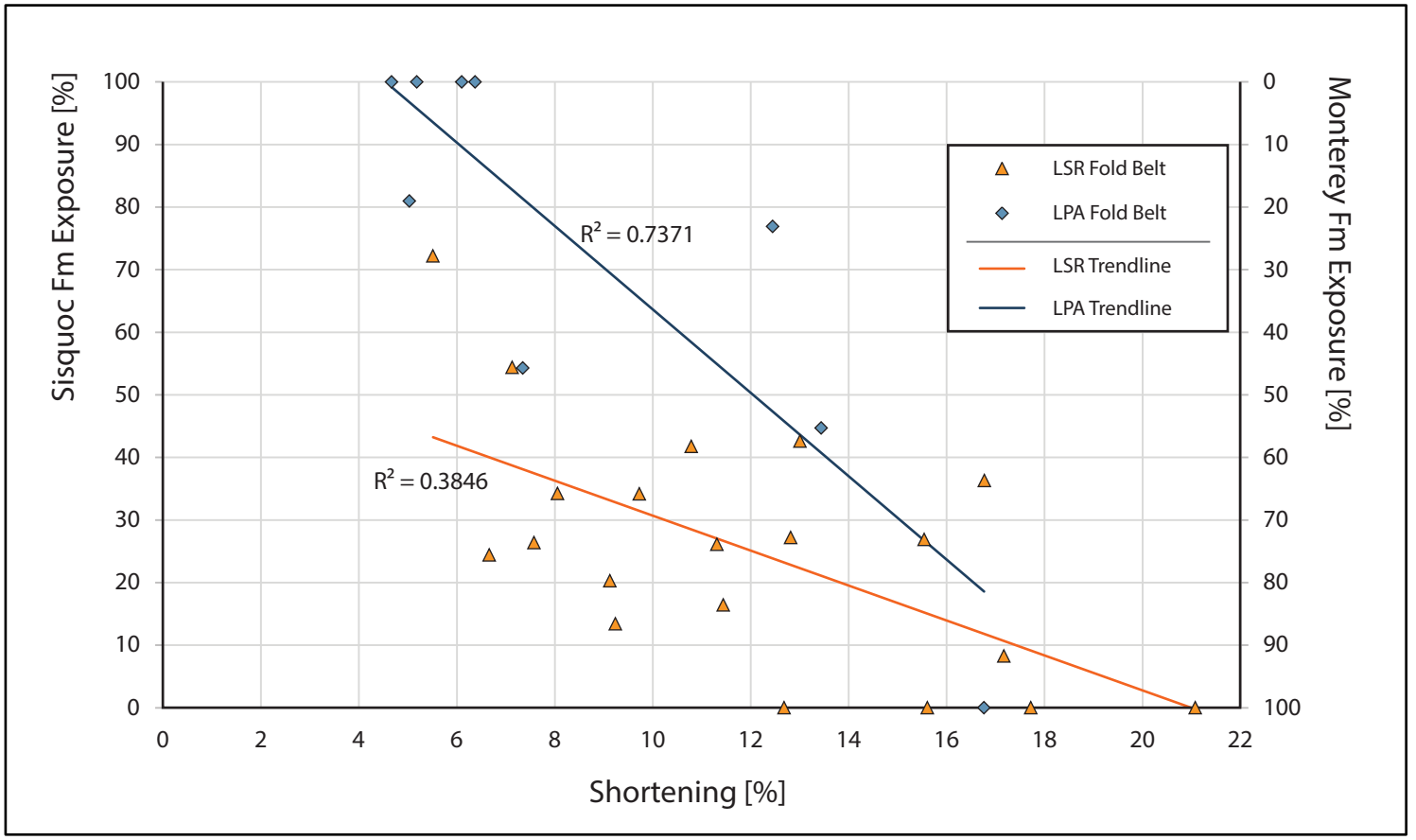

FIGURE 13. Correlation of the formational ratio (Sisquoc : Monterey) used during line-length-section construction over shortening results in LSR (orange) and LPA (blue).

shortening rates and transects with mostly Sisqouc exposures show the lowest shortening rates (Fig. 13).

Fold interlimb angles range from 55° to 171° in the LSR, 78° to 171° in the LPA (Fig. 14), with a mean interlimb angle of 113°. In the Sisquoc Formation, gentle folding predominates with 79 % in the LSR and 86% in the LPA (Table 2). Open folding is much less expressed by 19% in the LSR and 11% in the LPA. Only minor amounts of close fold angles are present in the Sisquoc - 2% in the LSR and 3% in the LPA (Table 2). In the Monterey Formation, fewer gentle folds are expressed with 49% in the LSR and 38% in the LPA (Table 2). Compared to the Sisquoc Formation, the Monterey Formation expresses more open folds, with 43% in the LSR and 57% in the LPA (table 2). Close fold angles are expressed in the LSR (8%) and in the LPA (5%) (table 2). The results show that the majority of fold angles are gentle in the Sisquoc Formation, and gentle to open in the Monterey Formation (Fig. 14; Table 2).

TABLE 2. Results for Measured Fold Angles in the Sisquoc and Monterey Formations

L S R	Sisquoc Formation	Monterey Formation
Gentle (171° - 124°)	79 %	49 %
Open (123° - 89°)	19 %	43 %
Close (88° - 55°)	2 %	8 %
L P A	**Sisquoc Formation**	**Monterey Formation**
Gentle (171° - 124°)	86 %	38 %
Open (123° - 89°)	11 %	57 %
Close (88° - 55°)	3 %	5 %

Note: Classified after Ramsay (1974)

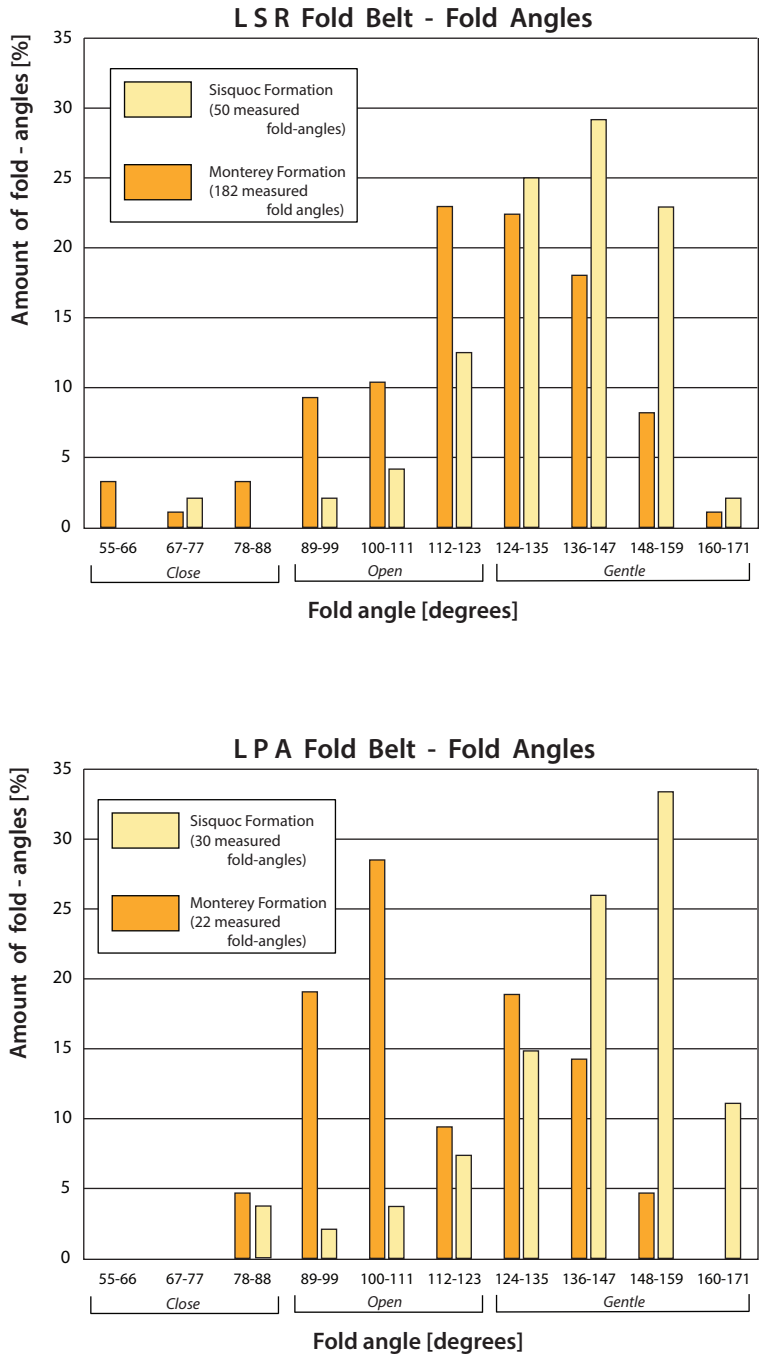

FIGURE 14. Histogram of fold-angles measured in the Sisquoc (beige) and Monterey (orange) formations for the LSR (top) and LPA (bottom). The fold angles are plotted against the percentage of total measured formation internal fold-angles.

Wavelength vs. amplitude was plotted for 49 folds for the Sisquoc Formation and 156 folds for the Monterey Formation in the LSR. In the LPA, wavelength vs. amplitude was plotted for 28 folds in the Sisquoc Formation and 19 folds in the Monterey Formation. The results show a positive linear correlation between the wavelength (W) and amplitude (A) for both the Sisquoc and the Monterey Formation (Fig. 15). The average wavelength vs. amplitude in the Monterey Formation is about twice as high as in the Sisquoc Formation in the LSR and LPA (Table 3). In the LSR, the average wavelength in the Sisquoc Formation is 1.02 km (with a range of 0.16 km to 4.08 km) and 0.86 km in the Monterey Formation (with a range of 0.11 km to 4.34 km) (Fig. 15). The fold amplitude average is 0.13 km in the Sisquoc Formation (with a range of 0.02 km to 0.57 km) and 0.23 km in the Monterey Formation (with a range of 0.04 km to 0.83 km) (Fig. 15 a). In the LPA, the average wavelength in the Sisquoc Formation is 1.84 km (with a range of 0.17 to 3.79 km) and 0.83 km in the Monterey Formation (with a range of 0.27 km to 2.0 km) (Fig. 15). The fold amplitude average is 0.24 km in the Sisquoc Formation (with a range of 0.06 km to 0.55 km) and 0.26 km in the Monterey Formation (with a range of 0.06 km to 0.61 km) (Fig. 15).

TABLE 3. Slope Function for Wavelength (W) vs. Amplitude (A) for the LSR and LPA

	Sisquoc Formation	Monterey Formation
L S R	$A = 0.14 \times W$	$A = 0.24 \times W$
L P A	$A = 0.12 \times W$	$A = 0.29 \times W$

Similarly, a positive linear correlation between the amplitude and the fold shortening is observed for both the Sisquoc and the Monterey Formations (Fig. 16). In the LSR and in the

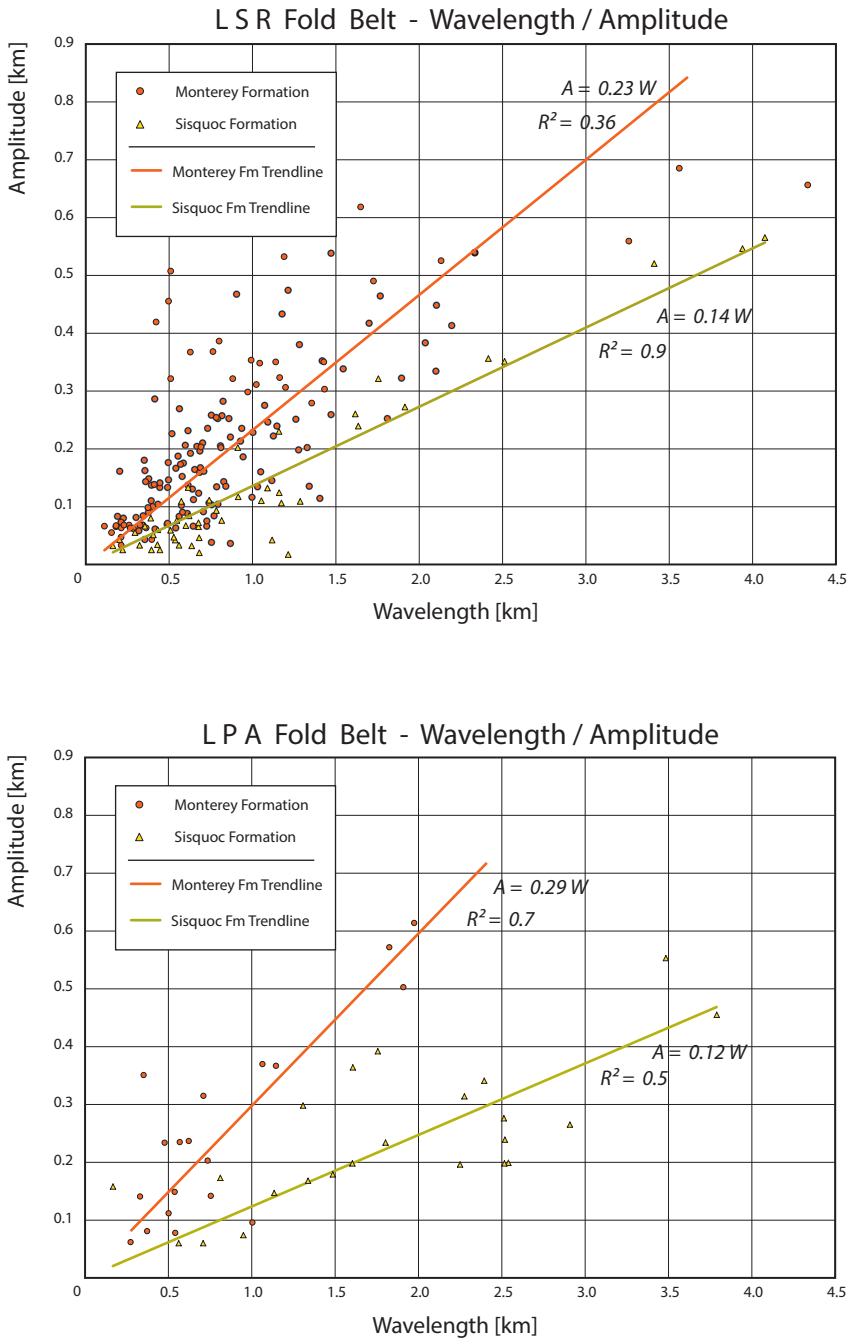

FIGURE 15. Correlation of fold wavelength against fold amplitude for the Sisquoc Formation (yellow) and Monterey Formation (orange) folds in the LSR (top) and LPA (bottom).

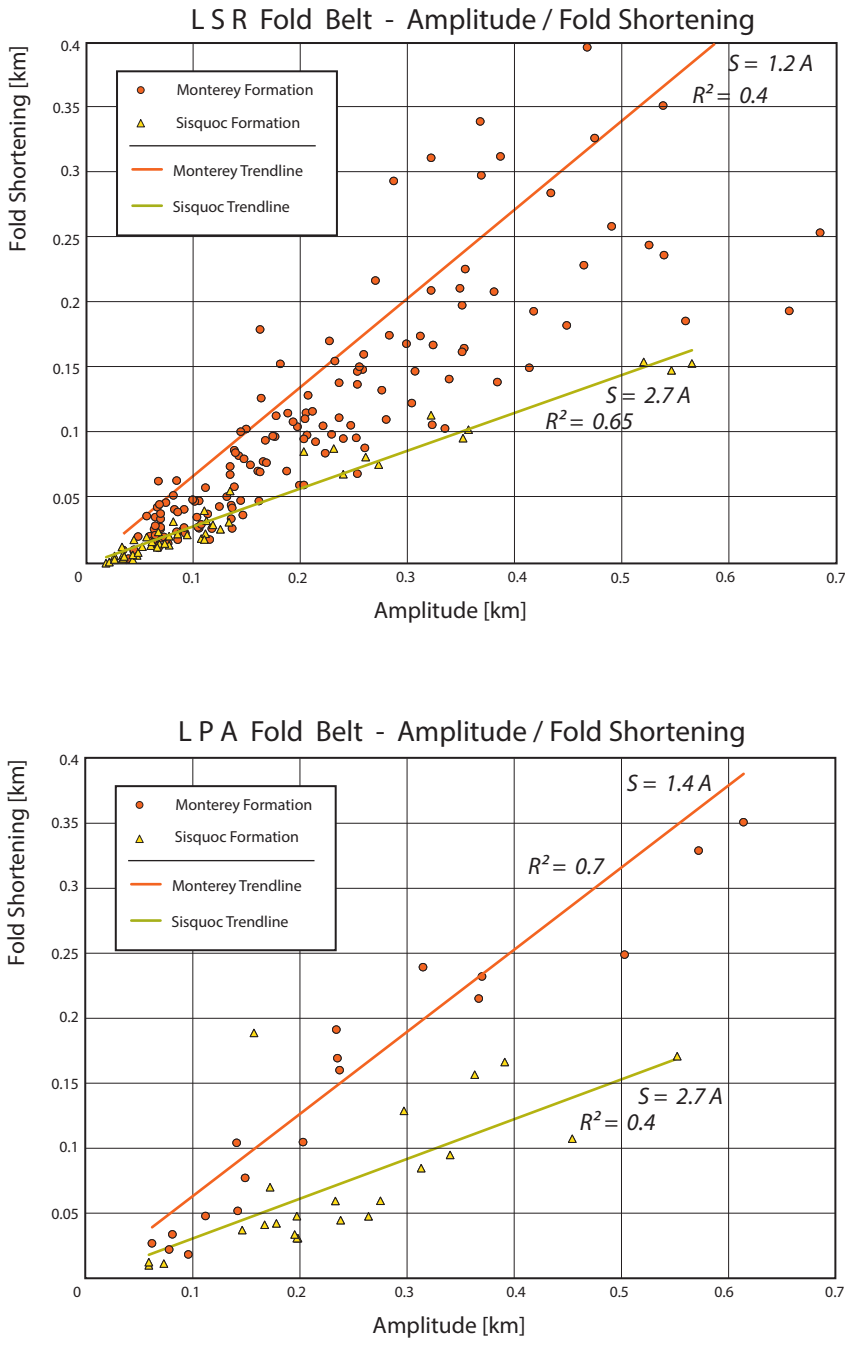

FIGURE 16. Correlation of fold amplitude against fold shortening the Sisquoc Formation (yellow) and Monterey Formation (orange) folds in the LSR (top) and LPA (bottom).

LPA, the amplitude to shortening slope function shows that the amplitude is twice as high in the Monterey Formation compared to the Sisquoc Formation (Table 4). This coincides with the results for the general shortening ratios between the Sisquoc Formation and the Monterey Formation (Table 1). Therefore, fold shortening is accommodated about twice as much in the Monterey Formation than in the Sisquoc Formation.

TABLE 4. Slope Function for Amplitude (A) vs. Fold Shortening (FS) for the LSR and LPA

	Sisquoc Formation	Monterey Formation
L S R	$FS = 0.27 \times A$	$FS = 0.12 \times A$
L P A	$FS = 0.27 \times A$	$FS = 0.14 \times A$

CHAPTER 4

OUTCROP-SCALE FOLD STRAIN ANALYSIS

Purpose and Selection of Outcrops

The upper, thinly bedded siliceous member of the Monterey Formation displays intraformational deformation at outcrop-scale including a variety of different types of detachment folds and fault-propagation folds (Snyder, 1987) that are interpreted to be the result of blind thrusts splaying off detachment horizons at depth, and bedding-plane detachments themselves are folded progressively during deformation (Gutiérrez-Alonso and Gross, 1996). In this study, documentation of outcrop-scale structures and structural mapping of Sisquoc and upper Monterey Formation outcrops was done in reference to the map-scale structures in order to (1) better understand the deformation mechanisms at outcrop-scale, (2) analyze if structures and deformation mechanisms at this scale vary as a function of mechanical stratigraphy and map-scale structural position, (3) investigate if strain related to the outcrop-scale is additive to the map-scale, and (4) obtain constraints on the timing of outcrop-scale deformation relative to the map-scale deformation. Structural mapping was performed at San Miguelito Canyon and Sweeney Road, near Lompoc, California (Fig. 9). The structures at both sites are well suited targets for this study because of excellent exposure, a variety of map-scale structural domains to test the influence of structural position, a variety of interbedded rocks with contrasting competence ranging from porous diatomite to competent chert/porcelanite to test the influence of mechanical stratigraphy, and outcrop orientation perpendicular to map-scale fold strike. The outcrops at San Miguelito Canyon are located along the western side of the canyon (Fig. 9, Fig. 17).

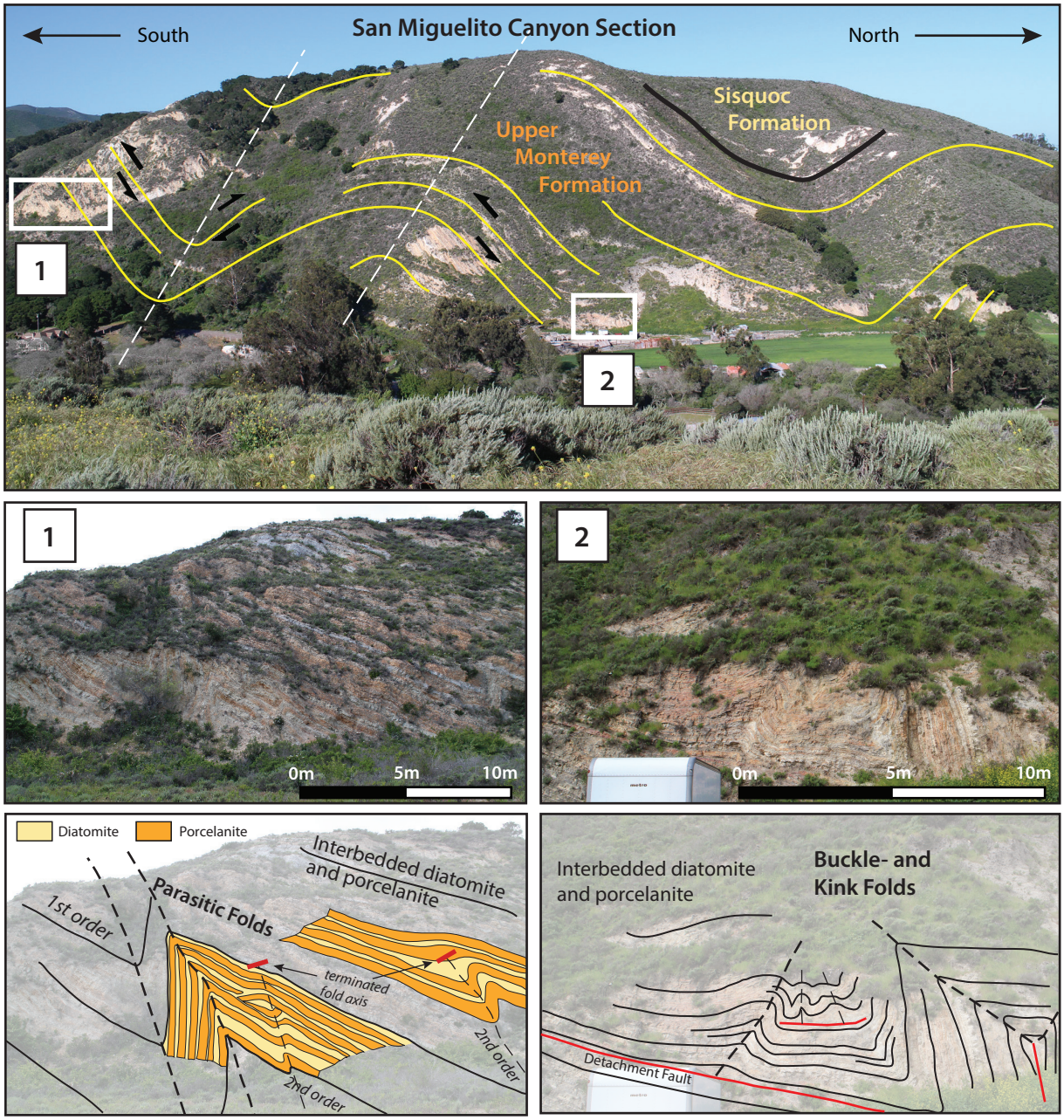

FIGURE 17. Image of a well-exposed and deformed section of the upper Monterey Formation at San Miguelito Canyon (top picture). White dashed line showing general map-scale structural setting with a syncline to the south and an anticline just to the north (bedding planes shown in yellow). The outcrop structures are within map-scale folds. Structures are parasitic folds (Box 1) and buckle and kink folds (Box 2). In general these types of structures are located in the limbs of the tight folds.

Exposure at Sweeney Road is much better and located along a road cut within a nearly vertical cliff of the meandering Santa Ynez River as part of a cut bank (Fig. 9, Fig.18). The cut bank in combination with the road cut created a 500 meters long, 80 meters high, well-exposed outcrop (Fig. 18). Outcrop mapping was done in high detail at Sweeney Road because of better exposure and better control on stratigraphic data.

Methods

Because the outcrop structures are tested to be a function of lithology and structural position, it was important to create an accurate outcrop map that integrates data regarding the mechanical stratigraphy, the map-scale structures, and outcrop-scale structures. The sections at San Miguelito and Sweeney Road were chosen to document the style and lithologies of outcrop-scale structures and their structural position at map-scale. The section at Sweeney Road provides much better exposure and was chosen to create an accurate map to also document the mechanical stratigraphy throughout the section. This was accomplished by creating an orthoimage of 150 images covering most of the outcrop (Fig. 18 - outlined in red). Unlike an uncorrected image, an orthoimage can be used to measure true distances because it is adjusted for relief, lens distortion, and camera tilt. Therefore, the image is geometrically corrected such that the scale is uniform. In a second step, the image orientation was corrected according to the orientation of regional strike that was taken from bedding plane measurements along the outcrop. In a third step, the orthoimage was loaded into LithoTect in order to use structural projection tools and establish a structural framework to tie the outcrop-scale structures with the map-scale. In a last step, the image was loaded into Adobe Illustrator to place detailed line work of the bedding planes and structures, and illustrate mechanical stratigraphy along the outcrop (Fig. 19).

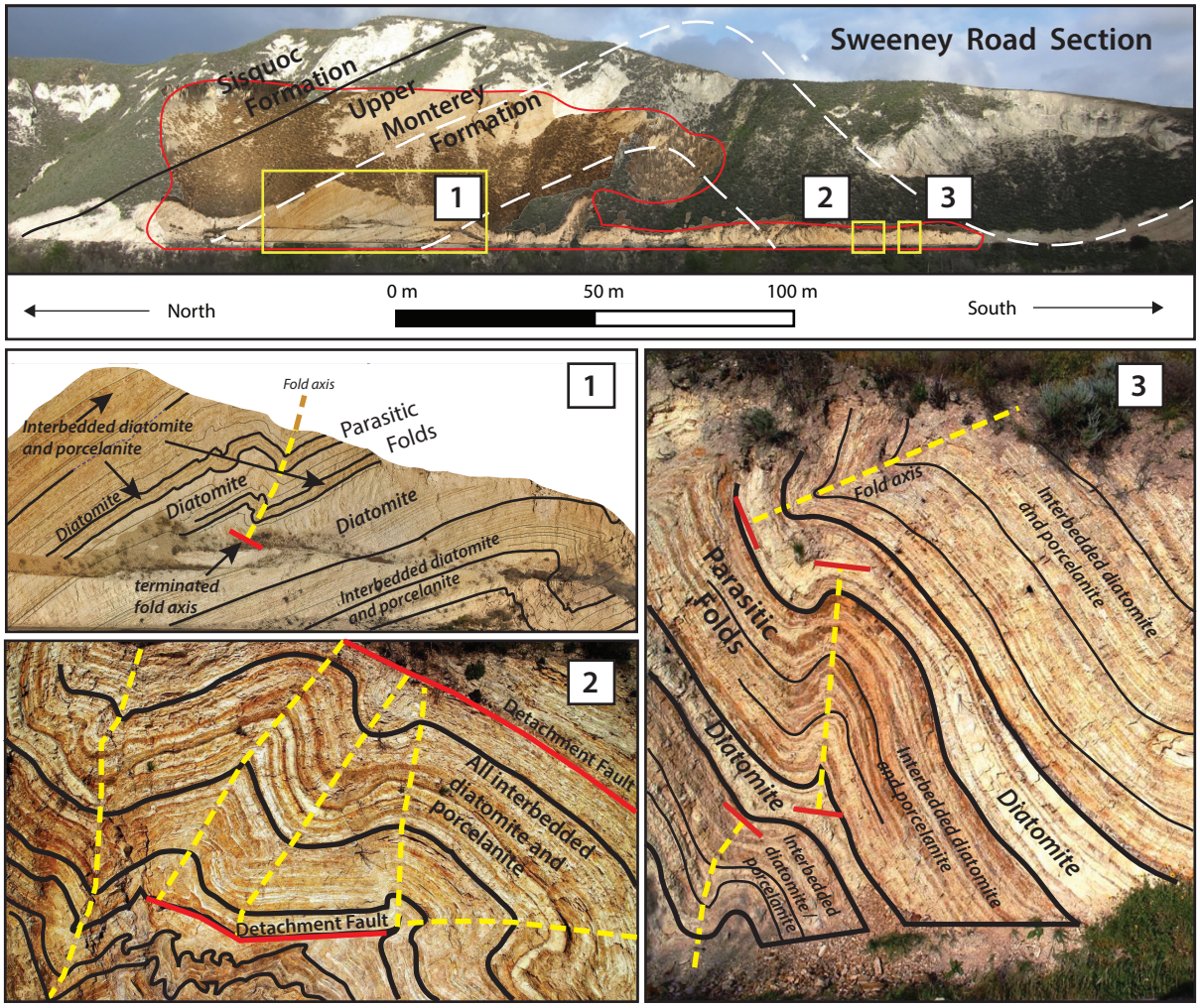

FIGURE 18. Image of Sweeney Road section and orthoimage (outlined in red) (top picture) that was used for outcrop-scale structural analysis. White dashed line showing general anticline/syncline pair geometry. Details of deformation are shown in boxes 1-3. Yellow dashed line showing fold axes of disharmonic parasitic folds that terminate within the diatomite dominated layers and disharmonic buckle folds that terminate at a detachment surface. Note the thickness variations in the diatomite layers in (1) and (3).

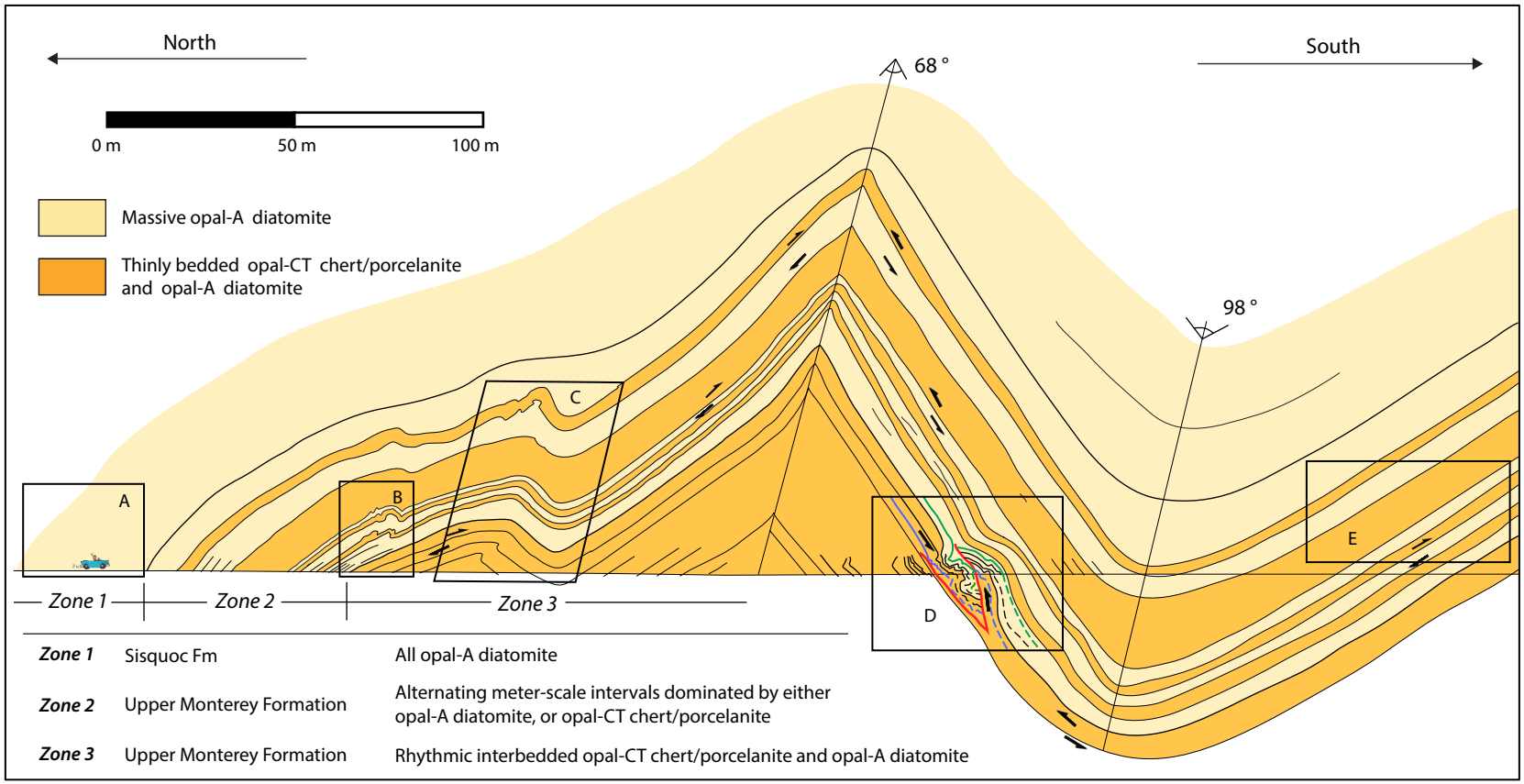

FIGURE 19. Map of fold structures of the Sisquoc Formation and upper Monterey Formation at Sweeney Road. Boxes A-E show the different structural styles including massive beds (box A), disharmonic folds (box B), harmonic folds (box C), limb faults and buckle folds (box D), and pure flexural-slip (box E). Note that zones 1-3 exhibit a mechanical stratigraphy.

Field Descriptions

The investigated section at San Miguelito Canyon is folded into a syncline to the south, followed by an anticline to the north. The syncline/ anticline pair has close fold angles of 81° for the syncline and 78° for the anticline. Two exposures with extensive outcrop-scale folding were identified in the upper Monterey Formation (Fig. 17). The south-limb of the syncline exhibits parasitic folds with s-vergence (looking westward) of first and second order (Fig. 17 box 1) with centimeter-scale interbedded diatomite and porcelanite of approximately equal amounts. However, the diatomites show significant variations in bed thickness within the parasitic folds (Fig. 17 box 1.). The exposure on the north-limb of the adjacent anticline exhibits a variety of buckle folds and a box fold above a bedding plane detachment surface (Fig. 17, box 2). The outcrop also exposes centimeter-scale interbedded diatomite and porcelanite.

Strata at Sweeney Road is much better exposed and folded into an anticline to the north and a syncline to the south (Fig. 18, 19). The anticline/ syncline pair is folded into concentric and chevron type folds with fold angles of 68° for the anticline and 98° for the syncline, with steeply north-dipping axial planes (Fig. 19). Like San Miguelito Canyon, these fold angles are one of the tightest in the LSR. The two folds exhibit a steeply dipping anticlinal north-limb with no paired adjacent structure, a steeply dipping anticlinal south-limb and a moderately dipping synclinal south-limb with no paired adjacent structure (Fig. 19).

The Monterey and Sisquoc formations at Sweeney Road display variations in silica phases mainly from porous diatomites (opal-A) to more competent cherts and porcelanites (opal-CT) that provide variations in mechanical rock properties (Fig. 7, 8). The relative distribution of diatomite to chert/porcelanite changes progressively throughout the section with pure diatomite in the Sisquoc Formation to chert/porcelanite dominated intervals in the upper Monterey

Formation (Fig. 19). Three zones of distinct contrasting mechanical properties were identified. Zone 1 is in the lower Sisquoc Formation and mechanically homogeneous. The main lithology is diatomite. Zone 2 is the initial diagenetic transition zone in the upper Monterey Formation and is composed of alternating meter-scale intervals dominated by either diatomite, or chert/porcelanite (Fig. 19). Zone 3 exposes thinly bedded upper Monterey Formation that is characterized by rhythmic interbedded chert/porcelanite and more porous and detritus rich diatomaceous sediment (Fig. 19). The three identified zones are consistent with the three siliceous diagenetic stages that were explained in figure 8.

The most prominent outcrop-scale structures were investigated at five locations each with different mechanical and/or map-scale structural settings (Fig. 19 boxes A-E) in order to investigate their influence on the deformation. The first location (Fig. 19 box A) is located on the north-limb of the anticline and lithologically in zone 1 and composed entirely of diatomite of low competence. No outcrop-scale structures were observed within this domain. The second location (Fig. 19 box B) is structurally located on the north-limb of the anticline and is lithologically in a diagenetic transition zone with diatomite dominated to chert/porcelanite dominated rocks through the section (zone 2). The zone consists of alternating meter-scale intervals dominated either by chert/porcelanite and diatomite. The most prominent structures are Z-shaped folds with differing scales and wavelengths. Folds occur through the more competent beds that are dominated by cherts and porcelanites. The porous diatomite intervals are also displaced by the folds, but the folds vanish away from the folded chert/porcelanite dominated package (Fig. 18; Fig. 19 box B). Fold wavelengths differ depending on layer thickness. Thicker competent packages display longer fold wavelengths than the thinner competent packages in the more massive diatomaceous intervals (Fig. 19 box B and C). The third location (Fig. 19 box D) is

structurally located on the south-limb of the anticline and north-limb of the syncline). Lithologically it exposes a thick package of thinly-bedded chert/porcelanite dominated lithologies towards the center of the anticline (zone 3) and thinner packages of chert/porcelanite dominated lithologies within a thicker interval of incompetent diatomite towards the center of the syncline (zone 2). The largest and most prominent outcrop-scale structure within this domain is a low-angle (relative to bedding) limb thrust fault that transects a more competent section of chert/porcelanite dominated rocks and penetrates into the more incompetent section of diatomite dominated rocks via a hanging-wall cutoff. This geometry produced a variety of lower order folds and internal footwall buckle folds and a hanging wall fault-bend fold (Fig. 19 box D). The structural position of the fourth location is on the south limb of the syncline and inhabits zones 1-3. Similar to the first location, no major outcrop-scale structures were observed within this domain. Zones two and three, that are folded or faulted in the previous described locations show minor to no folding (Fig. 19 box E).

CHAPTER 5

DISCUSSION

A deformation model is presented based on detailed analysis of strain variations between mechanically homogeneous diatomite of the Sisquoc Formation and the thinly and mixed bedded diatomite and chert/porcelanite of the upper Monterey Formation. The model integrates observations made at map-scale and outcrop-scale and may have implications for assessing regional deeper subsurface geometries and kinematics.

Interpretation of Strain Differences Between the Sisquoc Formation and Upper Monterey Formation

Line-length-sections of the Sisquoc and upper Monterey formations in the LSR- and LPA fold-belts provide the critical constraint for analyzing and interpreting strain between the two units. Results show that measured shortening fluctuates up to 15.6% in the LSR and 12.1% in LPA, respectively, over sub-regional scale distances (Fig. 12, Table 1). The amount of measured shortening strongly relates to the predominant lithology of the formation that was used for structural data with high fold strain in the thin-bedded diagenetic rocks (porcelanite and chert) of the Monterey Formation and low fold strain in the diatomaceous Sisquoc Formation (Fig. 13, Table 1). Therefore, the geometry of the constructed line-length-sections is highly dependent on the lithology of the formation exposed at the surface. Fold geometries for both study areas show a higher heterogeneity in fold angles and generally tighter fold angles in the upper Monterey Formation (Fig. 14). The Monterey vs. Sisquoc shortening ratios (Table 1) and trend-line functions of amplitude over fold shortening plots (Fig. 16; Table 4) show shortening in the thin-bedded and more competent upper Monterey Formation to be twice as high as in the overlying, thick bedded, and less competent Sisquoc Formation.

Three possible scenarios may explain these strain and geometry variations. One possibility is an unconformity between the Monterey and the Sisquoc Formation. An uplift event during the late Miocene Rafaelan orogeny is documented through localized erosional unconformities at the base of the Sisquoc Formation in the San Rafael Mountains about 40 km to the north (Dibblee, 1950) and in the Santa Maria basin along many anticlines (Dumont and Barron, 1995). Although there is some evidence for localized vertical movement and erosion, there is no evidence for an unconformity at the two outcrop sections analyzed in this study (Fig. 17, 19) and no indication in the surface mapping of the study area for an unconformity (Dibblee, 1950; Dibble and Ehrenspeck, 1988a, 1988b, 1988c, 1988d, 1988e, 1993a, 1993b) that could discretely separate beds of different strain histories. Furthermore, most widespread shortening occurred after the deposition of the Sisquoc Formation (Dibblee, 1950). Therefore, the contact between the Sisquoc Formation and the Monterey Formation is probably conformable and tectonic shortening between both units is assumed to be relatively identical.

A second possibility is that the two units are separate structural systems and decoupled via a detachment fault. In this scenario the Monterey would undergo deformation by folding while the Sisquoc Formation would undergo less deformation with slip being consumed by a basal detachment fault instead of progressively folding in the Sisquoc Formation. Not supporting this explanation are map-scale fold axes staying consistent across the contact between Monterey and Sisquoc Formations without significant changes in orientation of bedding strike and dip. Furthermore, no regional detachment horizon between the Sisquoc and the Monterey Formations has been mapped by previous workers (Dibblee, 1950; 1988 a-e; 1993 a,b), or observed during fieldwork in this study.

A more likely third possibility relates to the different mechanical rock properties between the different siliceous diagenetic stages (Fig. 8). In the following, a new deformation model based on observation of the structural behavior of the different siliceous diagenetic stages during contraction will be presented. Siliceous sediments undergo significant mechanical modification with burial (Isaacs, 1981) (Fig. 7). In the study areas, diagenetic modification resulted in a thin-bedded, mechanically contrasting and more competent upper Monterey Formation, and a thick bedded, mechanically homogeneous, highly porous and less competent overlying Sisquoc Formation. Under otherwise identical tectonic conditions, different deformational styles result from rocks in different diagenetic states (Snyder, 1987). Strain quantification at outcrop-scale and micro-scale between different silica phases has already shown that the fold strain of competent chert/porcelanite intervals at outcrop-scale is much higher than fold strain of interbedded diatomites, but the missing fold strain (simple shear) is accommodated by layer-parallel strain (pure shear) in the diatomite (Behl, 1992). Therefore, strain between different silica phases can be recorded via different strain mechanisms so that their total shortening budgets still match. The deformation model presented here suggests that the same amount of strain was recorded by the upper Monterey and Sisquoc formations, but with different mechanisms. This strain is displayed by open to close folding and faulting in the brittle diagenetic rocks of the Monterey, but by horizontal compaction and gentle to open folding in the diatomaceous Sisquoc Formation (Fig. 14; Fig. 20). Therefore, total fold strain at sub-regional scales is best measured by restoring line-length-sections in the Monterey Formation because it is mechanically competent enough to respond to stress via folding and not horizontal

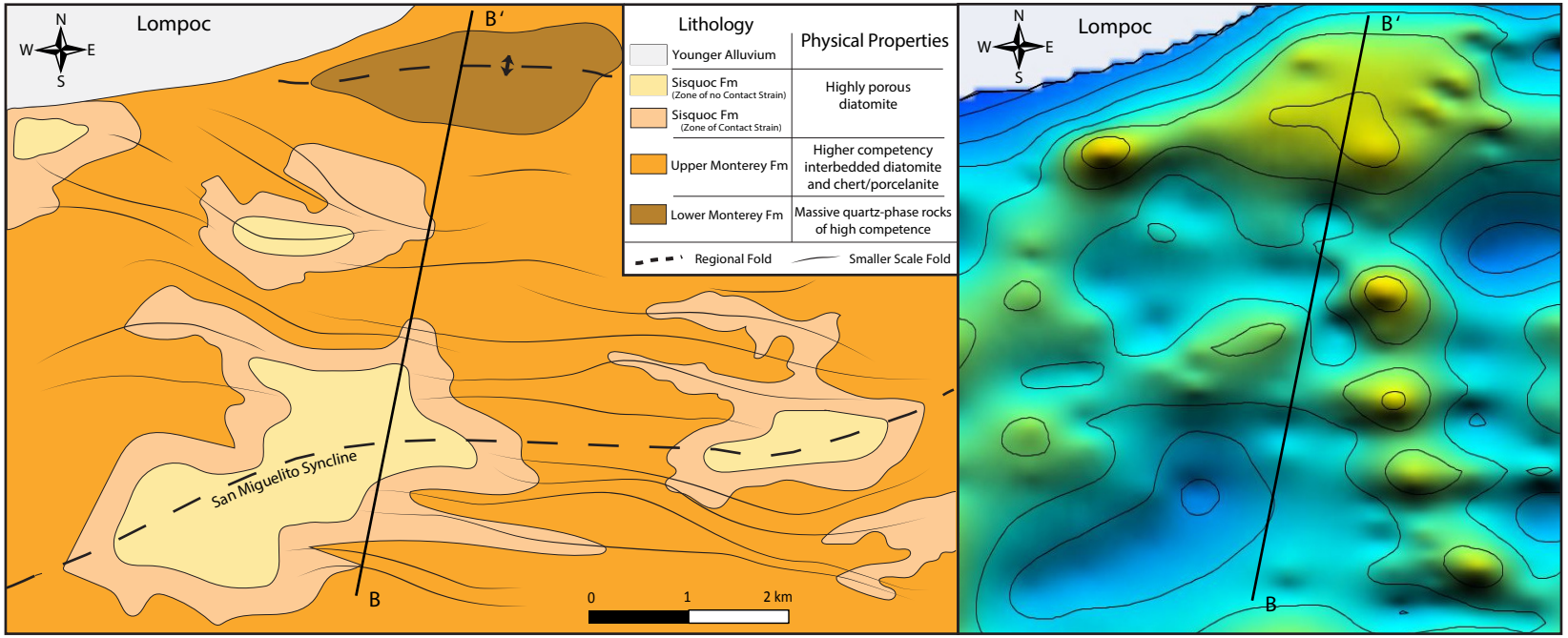
N
W
E
S
Lompoc
B'
B
San Miguelito Syncline
0
1
2 km
Lithology
Physical Properties
Younger Alluvium
Sisquoc Fm
(Zone of no Contact Strain)
Sisquoc Fm
(Zone of Contact Strain)
Highly porous diatomite
Upper Monterey Fm
Higher competency interbedded diatomite and chert/porcelanite
Lower Monterey Fm
Massive quartz-phase rocks of high competence
Regional Fold
Smaller Scale Fold

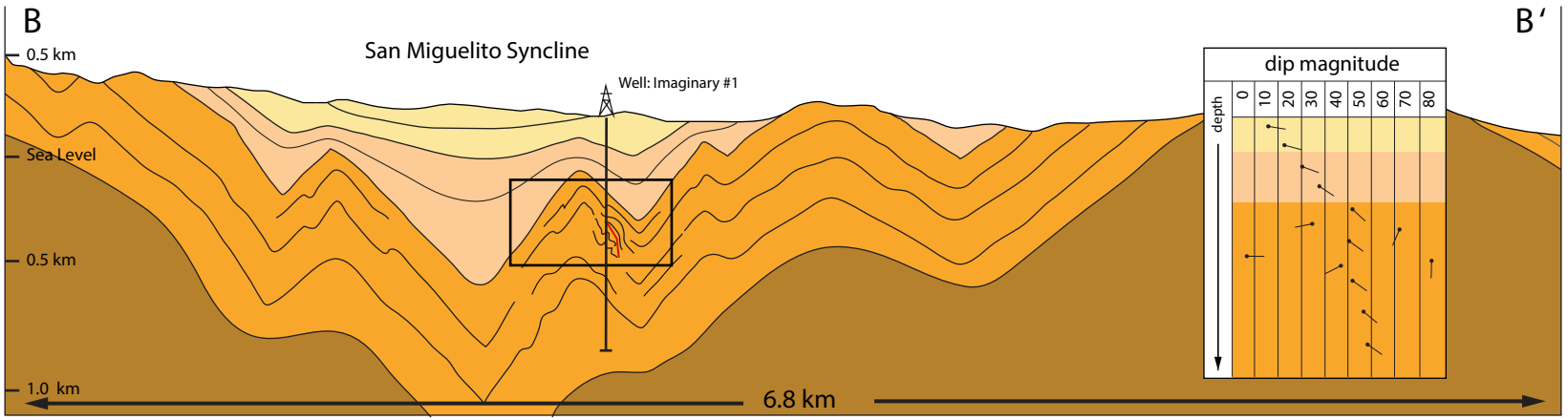
B
B'
San Miguelito Syncline
Well: Imaginary #1
0.5 km
Sea Level
0.5 km
1.0 km
6.8 km
dip magnitude
depth
0
10
20
30
40
50
60
70
80

FIGURE 20. Generalized geologic map (top left) (modified after Dibblee and Ehrenspeck, 1988a, 1988c, 1988d) and interpretation of deformation mechanisms (cross section B-B') in the Monterey and Sisquoc formations. Note the three different folding patterns developed across the geologic units: (1) close folding and outcrop-scale folding along limbs of tight folds in the upper Monterey (orange), zone of upper Monterey contact strain and open folding in the lower Sisquoc Formation (pink), and zone of no contact strain and broad folding in the upper Sisquoc Formation. Structure contour map of projected upper Monterey and Sisquoc contact (top right) created using line-length-sections 2-14. Note the tight folding in the areas of Monterey dominated surface data in the east and the broad to open folding in the areas of Sisquoc dominated surface data in the west. On the cross section an imaginary well predicts scattered dip magnitudes within high-angle limbs in the upper Monterey Formation that represent deformation at outcrop-scale.

compaction like the Sisquoc Formation. Representative sections for the Monterey Formation in the two study areas show 21.1% overall shortening in the LSR-, and 16.8% overall shortening in the LPA fold belt, respectively (Fig. 10, 12). A structure contour map from a representative area in the LSR fold belt was generated using the line-length-sections created in LithoTect (Fig. 20 - top right). The map shows short wavelength folds in areas with Monterey Formation surface exposure east of profile B-B' (Fig. 20). These folds vanish towards the west and transition up-section into a larger wavelength folds documented in the Sisquoc Formation exposed at the surface (Fig. 20). The structural style of tighter folding in the Monterey Formation should continue in the subsurface where covered by the Sisquoc Formation as shown in profile B-B' (Fig. 20).

The observations and interpretations made here show that significant fold strain variation can occur due to differences in rock rheologies at formational scale. This is expressed laterally along the surface by either climbing up-section into the Sisquoc Formation or dropping down-section into the Monterey Formation (Fig. 20). The large observable strain contrast is due to the extreme difference in competence and rheology of the primarily diatomaceous Sisquoc Formation and the chiefly cherty/porcelanitic Monterey Formation. The strain contrast effect on the construction of cross-sections would be much smaller in non-siliceous rocks with smaller competency contrast. This highlights that competence contrasts of geologic units can be an important component in constructing and assessing models in fold and thrust belts. Assessing the impact of competence contrasts in different geologic units on shortening measurements might revise some models of fold and thrust belts. This is likely to be more influential in fold-and-thrust belts across sedimentary basins with competence contrasting geologic units compared to thrust belts in more uniform strength rocks. The assessment of rock competence needs to be

incorporated into the construction of balanced cross-sections across fold-and-thrust belts developed in sedimentary basins.

Interpretation of Outcrop-Scale Structures

Surface strike and dip data were used to construct fold geometries in the Sisquoc and upper Monterey formations. This provided a useful first approximation of strain and support for a new deformation model (Fig. 20). Outcrop-scale structural analysis was performed in order to (1) analyze if structures and fold mechanisms at this scale vary as a function of mechanical stratigraphy between competent chert/porcelanite beds and incompetent diatomite, and map-scale structural position, (2) investigate if strain related to the outcrop-scale is additive to the map-scale, and (3) obtain constraints on the timing of its deformation and role to the map-scale deformation.

Observations of outcrop-scale structures of the competence contrasting siliceous sedimentary rocks of the Sisquoc and upper Monterey formations were made in anticline/ syncline pairs at San Miguelito Canyon and Sweeney Road, near Lompoc (Fig. 9, 17, 18, 19). In the upper Monterey Formation a variety of structures and deformational styles are observed. The most common structures are parasitic S- and Z-type folds along the limbs of the folded anticlines and synclines (Fig. 17, 18, 19). At Sweeney Road, parasitic folds with Z-type vergence (looking east) were observed on the north-limb of a map-scale anticline (Fig. 19, box B and C). There are many lower order parasitic S-type folds on the south-limb of the anticline (Fig. 18) and an out-of-the-syncline thrust fault intersects the S-type folds. This thrust fault is the dominant counter clockwise shear structure on this limb (Fig. 19, box D). It is interpreted to detach from a competent section of dominantly interbedded chert/porcelanite and diatomite, and penetrates into an incompetent section of dominantly diatomite via a hanging-wall cutoff. This produced a

domain of lower order buckle folds in the footwall and a hanging-wall fault-bend fold (Fig. 19, box D). The fault and fault related folds likely developed here instead of parasitic S-type folds. Buckle folds were also identified at San Miguelito Canyon (Fig. 17). These buckle folds are located at a similar structural position as the ones at Sweeney Road in between a pair of tightly folded synclines and anticlines (Fig. 17, 18, 19). Slip within these locations is transported via the bedding plane detachment faults out of the map-scale fold hinges creating a high strain situation expressed by small faults and buckling of the thinly bedded upper Monterey Formation instead of progressive folding. However, the parasitic folds and fault-related buckle are the result of shear decoupling mechanisms during flexural-slip deformation along the bedding planes. Therefore, the shear direction of parasitic folds and fault-related folds suggest that outcrop-scale folding occurred during map-scale folding and that fold and fault strain at outcrop-scale resulted from shear decoupling is not additive to the total strain at map-scale.

On the south limb of the syncline at Sweeney Road and along the remaining exposures along the section at San Miguelito Canyon, no outcrop-scale structures were observed (Fig. 17 and 19 box E). These sections are representative of the majority of the exposures in the upper Monterey Formation throughout the LSR. Field work identified only few locations with outcrop-scale structures. Both the Sweeney Road section and the San Miguelito Canyon section are located within the tightest folds across the entire LSR in the upper Monterey Formation. The outcrop-scale structures are not pervasive and probably only occur along the tight map-scale fold limbs where diatomite and chert/porcelanite coexists in thin beds and alternating packages of different thickness (Fig. 17, 18, 19). Dip-magnitudes of wells drilled through the tightly folded upper Monterey Formation are predicted to display inconsistent dip-angles that represent the deformation at outcrop-scale (Fig. 20). Therefore, regional structural subsurface modelling

requires caution in picking representative dip-angles from dip-meters that transect tightly folded upper Monterey Formation. In gently folded sections the dip-meters are expected to be consistent.

On the north-limb of the anticline at Sweeney Road and at the south-limb of the southern syncline at San Miguelito Canyon, parasitic folding is both harmonic, and disharmonic (Fig. 17, Fig. 18, and 19 box B). This is interpreted to result from different deformation mechanisms (simple shear of the chert/porcelanite dominated interbeds and pure shear of the diatomite dominated packages) bedding thickness, and interbedded competence-contrasting beds. There are two situations that develop harmonic and disharmonic folding. First, under the influence of flexural-slip deformation along the bedding planes, thinly interbedded chert/porcelanite dominated intervals can develop disharmonic folds above a bedding plane detachment (Fig. 17, 18). Slip on the detachment surface provides the fold shortening to the higher beds and the fold axis terminates downward into the detachment. If no detachment surface is present, folding becomes harmonic without termination of the fold axes (Fig. 17, 18). Secondly, if competent chert/porcelanite dominated interbeds are separated by a sufficiently thick and incompetent diatomaceous mechanical layer, the fold vanishes and the individual competent interbeds behave mechanically detached from each other and develop their own dominant wavelength without a fault separating the individual folds (Fig. 17, 18, 19). This is accompanied by significant thickness variations and fold termination through the diatomite layers (Fig. 17, 18). If competent chert/porcelanite dominated interbeds are separated by a relatively thin incompetent mechanical layer, but in close proximity to each other relative to their own thickness, then the fold of the competent interbeds reaches the next package of competent interbeds and the folding becomes harmonic (Fig. 19 box C). This interpretation suggests a relationship between the magnitude of

folding in the deformed chert/porcelanite dominated intervals and the thickness of intervening diatomite intervals that depends on how much local compaction can be absorbed by the diatomite without having to displace it. As a consequence, very small amounts of buckling can be harmonic between individual beds separated by only centimeters, but as the amplitude of folds increases, thicker stratigraphic units of porous diatomite would be required to keep folding from becoming harmonic. Therefore, in zone 2 (Fig. 19), folding within a thinly interbedded chert/porcelanite dominated interval tends to be harmonic because of the thin diatomaceous interbeds, but folding becomes disharmonic as subsequent packages of thinly bedded chert/porcelanite can be folded in an out-of-phase geometry because of the thick, intervening beds of diatomite (Fig. 17, 18, 19 box B and C). The deformation of incompetent layers that undergo folding as a result of the folding of adjacent competent layers has been described as contact strain (Frehner, 2008). In incompetent rocks with sufficient distance from the main fold, the folding becomes negligible and simple shear translates into pure shear and no contact to fold strain.

The documented deformation mechanisms (pure shear and simple shear) at outcrop-scale suggest that the mechanical stratigraphy is the main controlling element for decoupling along the Sisquoc- to upper Monterey Formation diagenetic boundary. The existence of zones within incompetent diatomaceous packages that translate fold strain into volumetric strain (zones of contact strain into zones of no contact strain) detach the fold strain at outcrop-scale and provide an explanation for how the distinct deformational styles between the purely diatomaceous Sisquoc Formation and the thin-bedded chert/porcelanite dominated upper Monterey Formation can exist without a detachment fault between them at formational scale (Fig. 20). The estimated fold geometries (Fig. 15; Table 2) and amplitude/wavelength ratios (Fig.16) show that even in

the primarily diatomaceous Sisquoc Formation, folds become tighter and amplitude/wavelength ratios increase with lower stratigraphic position in closer contact to the upper Monterey Formation. At outcrop-scale, this relationship is shown to be related to contact strain transmitted upwards from the underlying Monterey folding. Therefore, the map-scale structural style in the study areas progressively changes up-section from open to close, sub-regional folding in the upper Monterey Formation, to zone of contact strain folding in the lower Sisquoc Formation, to regional folding with no contact strain in the upper Sisquoc Formation (Fig. 20).

Implications for Structural Assessment of the Greater SMB Tectonic Province

Namson and Davis (1990) developed a structural model for the late Cenozoic regional deformation across the SMB and Western Transverse Ranges (Fig. 3). Deformation is interpreted to be the result of fault-bend and fault propagation folds developed above thrust ramps that step up from a regional detachment at 11-14 km depths. Their model has important implications for assessing the kinematic history of the entire SMB, its seismic hazards, and identifying petroleum traps. The Namson and Davis cross-section across the study area transects both the LSR- and LPA fold belts (Fig. 10). In the LSR, they used surface bedding strike and dips of the upper Monterey Formation, and subsurface data from one well with dip data along the northern flank of the fold belt to constrain fold geometries and the top Monterey line-length (Fig. 10). This part of their section measures 6.8% total fold shortening (Fig. 10 and 12; Table 1). In the LPA the fold geometries and top Sisquoc Formation line-length have been constrained by using surface bedding strike and dips of the Sisquoc Formation and subsurface data from 4 wells that have dip magnitudes. Namson and Davis measured 6.2% total fold shortening in this part of the section. In this study, fold shortening results from sections located adjacent to the Namson and Davis (1990) section coincide with the results by Namson and Davis: 6.7% shortening was measured in profile

16 in the LSR and 6.4% shortening was measured in profile 22 in the LPA (Fig. 12). In contrast, this study measured up to 21.1% shortening along profile 10 in the LSR, and 16.7% shortening along profile 28 in the LPA (Fig. 12). These ratios were calculated from transects that covered only Monterey dip data, as opposed to a mixture of Sisquoc and Monterey data. Therefore, the fold strain by Namson and Davis (1990) in the study area might be significantly underestimated. The following paragraphs discuss how additional fold strain measured in the Monterey Formation can be incorporated to the regional strain picture.

Two scenarios can explain how the difference in strain between the regional-scale and the map-scale can be balanced throughout the southern SMB structural province, how it might affect deeper subsurface structural interpretation, and what the implications are for assessing regional strain components and seismic risk. The first scenario assumes no change in subsurface kinematics and geometries as interpreted by Namson and Davis (1990) (Fig. 3). No additional strain can be consumed by folding or fault slip along deep detachments or thrusts. In order to match the strain budgets, the only solution to balance the amount of fold strain found in the upper Monterey Formation is to incorporate the same amount of layer-parallel strain into stratigraphic units below and above the upper Monterey Formation. This study showed that the predominantly diatomaceous rocks of the Sisquoc Formation have the potential to accommodate the missing fold strain primarily via volume reduction due to horizontal compaction. In the Ventura basin, it has been shown that penetrative deformation can contribute significant shortening and that this type of strain needs to be incorporated into the construction of balanced cross-sections (Duebendorfer and Meyer, 2002). Similar studies need to be done on geologic units below the Monterey Formation where fewer folds with greater wavelengths occur (Fig. 6) to determine if layer-parallel strain is significant enough to balance the additional fold strain.

A second scenario considers the possibility of a regional detachment fault at or near the base of the Monterey Formation in order to balance its additional fold strain. A detachment is the favored scenario because outcrop-scale structural analysis in this study has shown numerous detachment fault surfaces within the thin-bedded Monterey Formation rocks at many scales. Therefore, the likelihood for a regional detachment surface due to significant lithologic differences between the thin-bedded highly siliceous Monterey Formation and the older units (volcanics, sandstones, and silty shales) is very high. A detachment fault at the base of the Monterey Formation would have important implications with regard to emplacements of regional thrusts because significant amounts of slip need to be incorporated and balanced throughout the southern SMB tectonic province. In this study, a tectonic wedge model provides a structural interpretation to connect the interpreted shallow crustal detachment at the base of the Monterey to deeper crustal thrust faults and detachments (Fig. 21). However, compared to the layer-parallel strain model described in the first scenario, this solution adds significant fault slip into the kinematic system, opening up the possibility that the region is dominated by shallower blind thrusts that might be seismogenic. The wedge model (Fig. 21) also presents an interpretation for the geometry of a fault that has been identified using geologic maps (Hall, 1982) and well data (Fig. 21). A fault is mapped and recorded in the Rothschild #1 well along an east-west trending fault line that was described as the Santa Ynez River fault (SYRF) (Dibblee, 1950) (Fig. 9). Characterizations of the geometries and kinematics of the SYRF are numerous (Dibblee, 1950; Sylvester and Darrow, 1979; Hornafius et al., 1986; Sorlien et al., 1999). Most interpretations of the SYRF suggest that it accommodated strike-slip during clockwise rotation of small crustal blocks within the

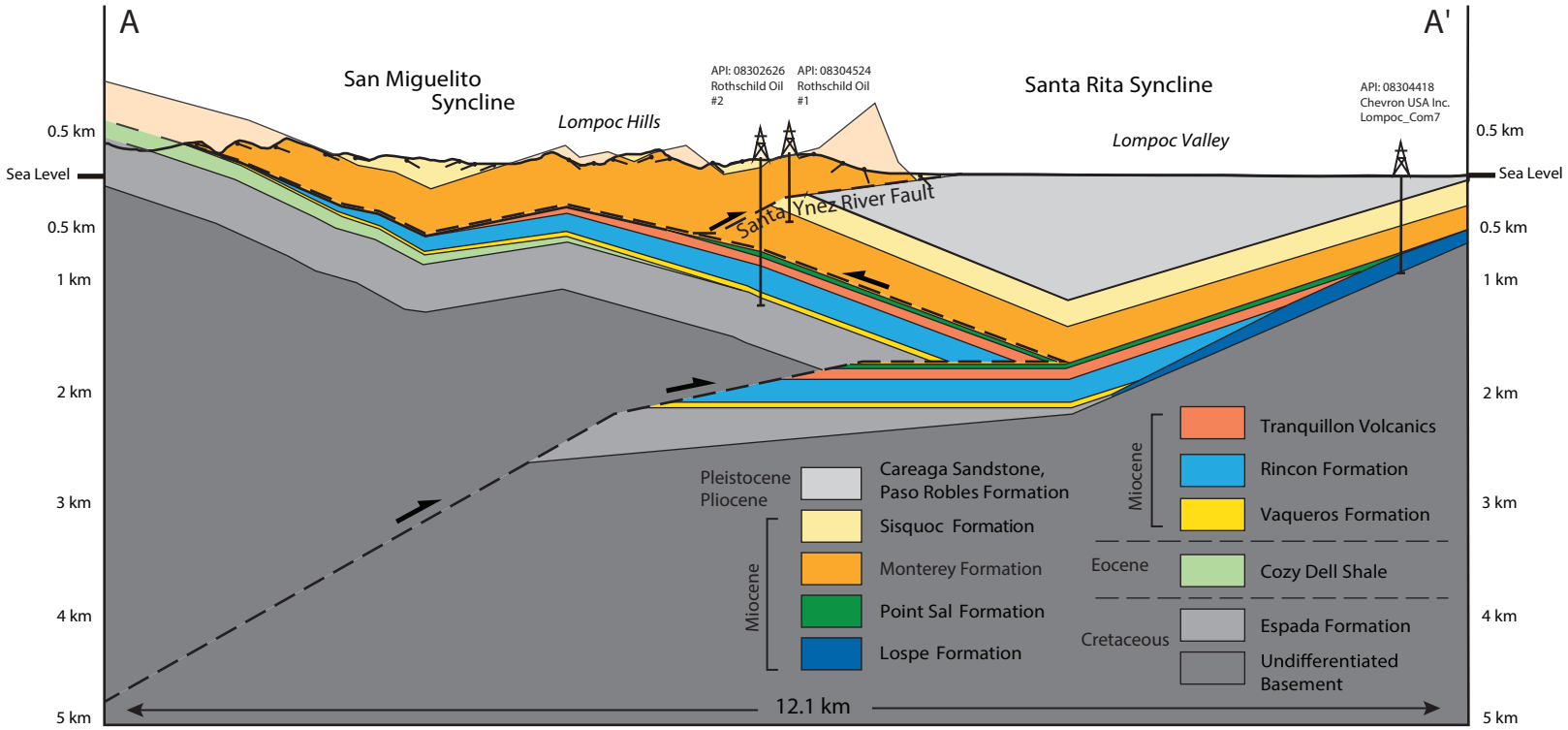

FIGURE 21. Tectonic wedge model tying the regional cross section by Namson and Davis (1990) with sub regional-scale deformation in the Monterey and Sisquoc Formations observed and measured in this study. The wedge links the shallow deformation to the deeper interpretation of Namson and Davis via low angle convergent faults and balances the additional shallow shortening observed and measured in the Monterey and Sisquoc Formations with the deeper-level shortening. This model assumes a detachment fault at the base of the Monterey Formation.

SMB (Hornafius et al., 1986; Sorlien et al., 1999). However, mapping shows significant north-south shortening in tight folds and steeply dipping beds along the Monterey/Sisquoc contact near the shallow position of the SYRF (Fig. 21). At this position fold angles are tight (below 60 degrees) as expected in hanging wall cutoff zones. This observation and the interpreted location of the fault (Hall, 1982) is used to constrain the dip of the SYRF by connecting the fault/well intersection in the Rothschild #1 well and its shallow location. As shown in Figure 21 the SYRF is a low-angle thrust and is interpreted to splay off a detachment horizon at the base of the Monterey Formation explaining the high shortening ratios and structural styles discussed in this study. This solution shows that the origin of the fault resulted from late Cenozoic north-south compression and not left-lateral strike slip as a resulting from ongoing clockwise rotation of internal blocks as suggested by Sorlien et al. (1999). The strain partitioning model (Namson and Davis, 1998b) probably better explains the regional strain picture, kinematics, and geometry of the SYRF. In order to test this interpretation, more detail on the SYRF geometry is needed along its trend from the study area to Lake Cachuma.

CHAPTER 6

CONCLUSION

Several key conclusions arise from strain analysis of the Monterey and overlying Sisquoc formations in the southern SMB.

1. Significant fold strain variation along strike can occur due to differences in rock rheologies at formational scale.
2. Mechanical stratigraphy is the main controlling element for decoupling along the Sisquoc- to upper Monterey Formation diagenetic boundary.
3. Parasitic folding at outcrop-scale is not pervasive and only occurs within tight map-scale anticline/syncline pairs. Its shear direction suggests that this deformation is coeval with the map-scale folding.
4. Thick diatomaceous intervals within stratigraphic sections can terminate the fold strain at outcrop-scale by transferring fold strain into volumetric compaction.
5. Distinct deformational styles can coexist in close proximity without a fault detachment between the purely diatomaceous Sisquoc Formation and the thin-bedded chert/porcelanite dominated upper Monterey Formation.
6. A tectonic wedge model provides a new subsurface interpretation to tie the additional shortening discovered in the Monterey Formation in this study with deep thrust faults as modeled by Namson and Davis (1990). This updated interpretation highlights the implications of sub regional scale strain analysis to the structural assessment of fold-and-thrust belts.
7. Strain analysis at outcrop-scale and subsurface interpretation at map-scale suggests a possible regional detachment fault at or near the base of the Monterey Formation.

8. A new 2D interpretation of the SYRF depicts a low-angle thrust geometry and a compressional origin of the fault.

APPENDIX

CONSTRUCTED CROSS-SECTIONS USED FOR STRAIN QUANTIFICATION IN THE

LOMPOC – SANTA ROSA FOLD BELT AND

LOMPOC – PURISIMA ANTICLINE FOLD BELT

Lompoc - Santa Rosa Fold Belt; Profiles 1 - 4

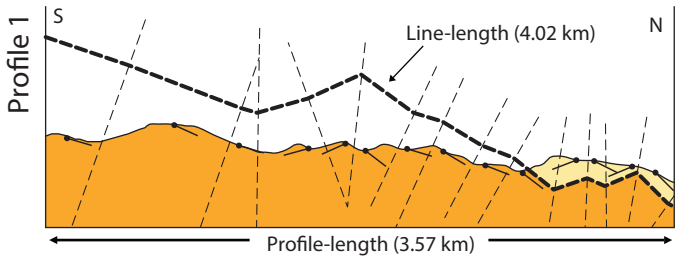

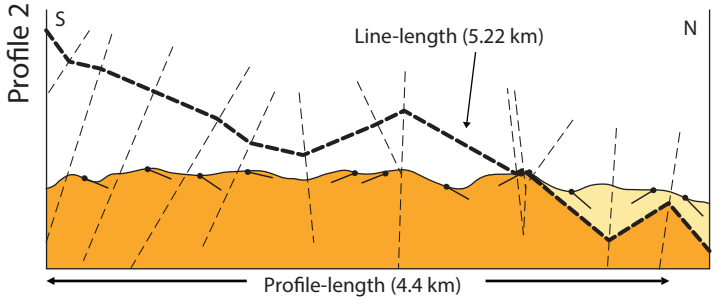

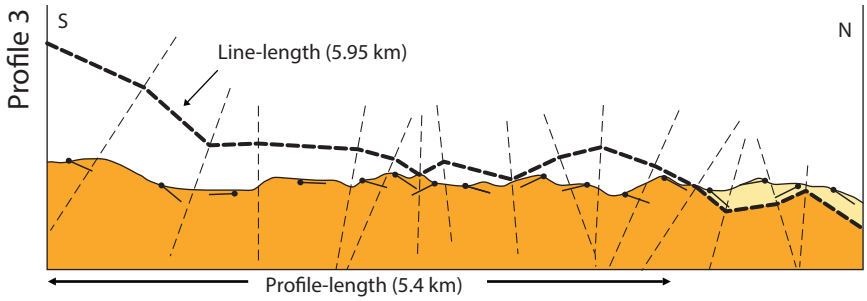

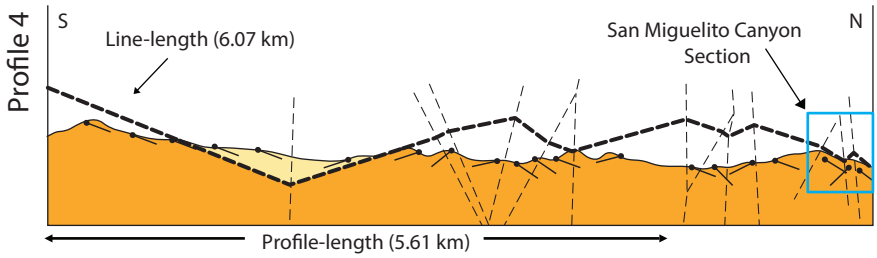

Lompoc - Santa Rosa Fold Belt; Profiles 5 - 8

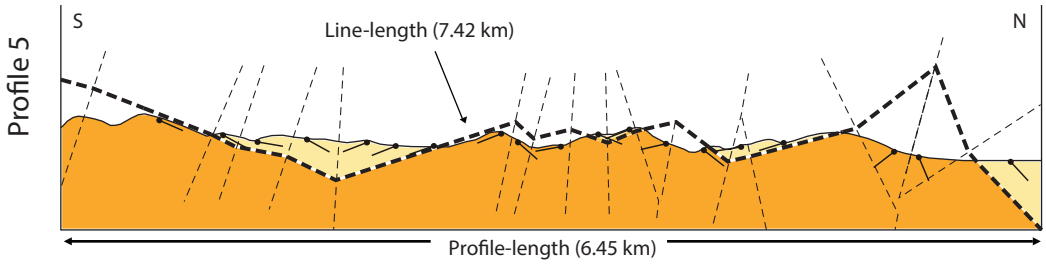

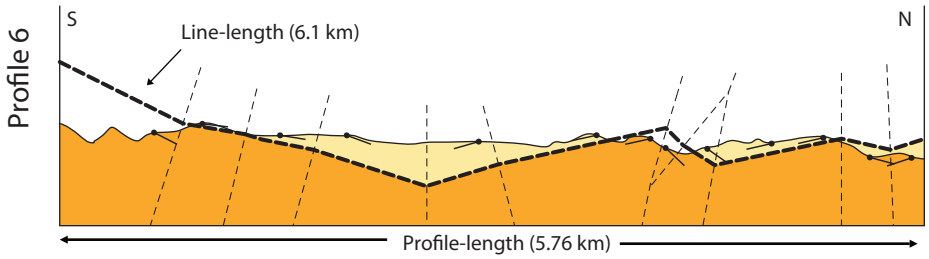

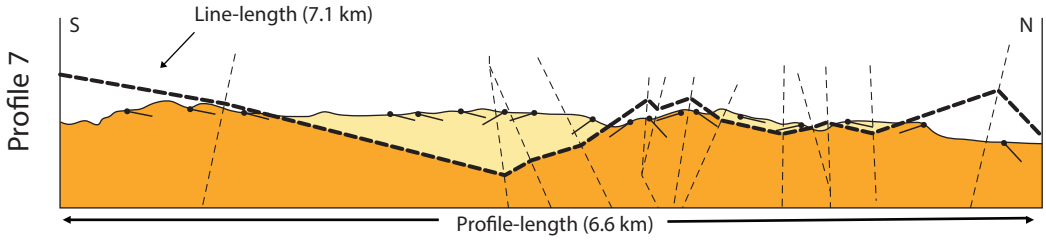

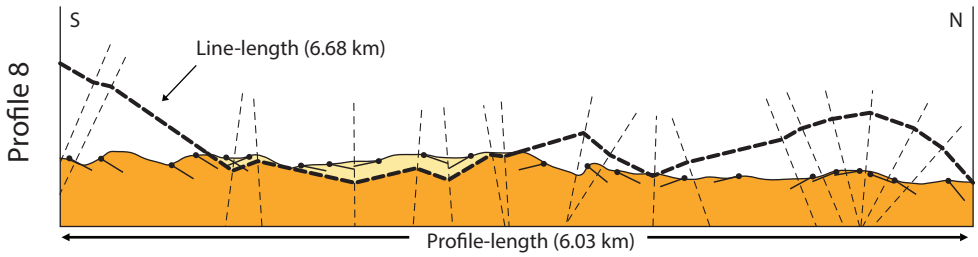

Lompoc - Santa Rosa Fold Belt; Profiles 9 - 12

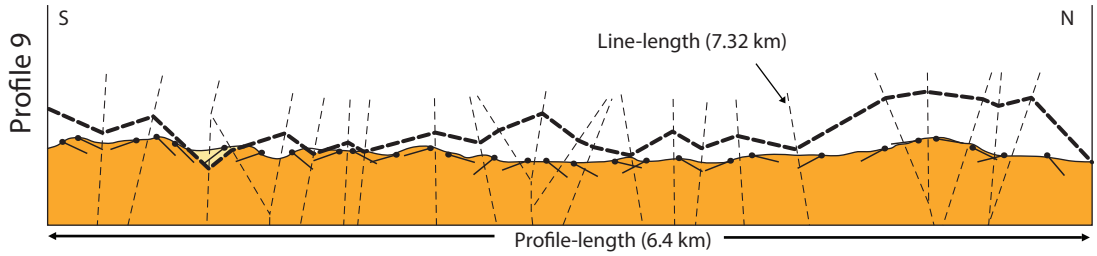

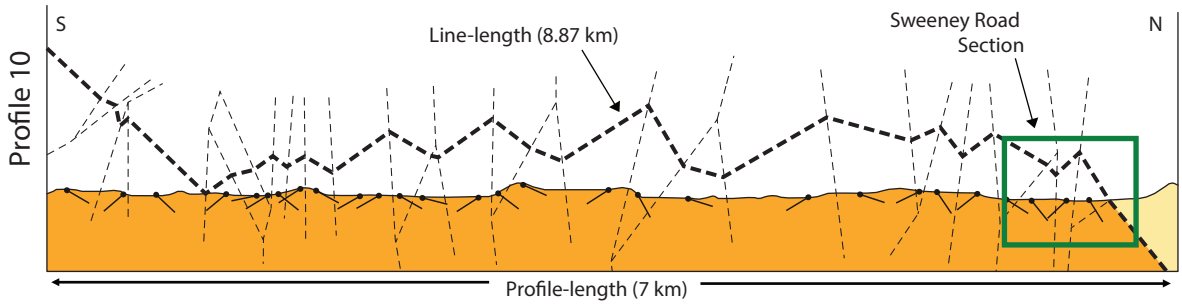

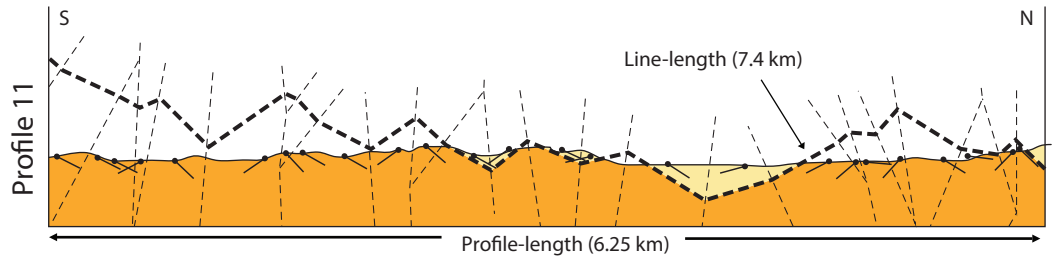

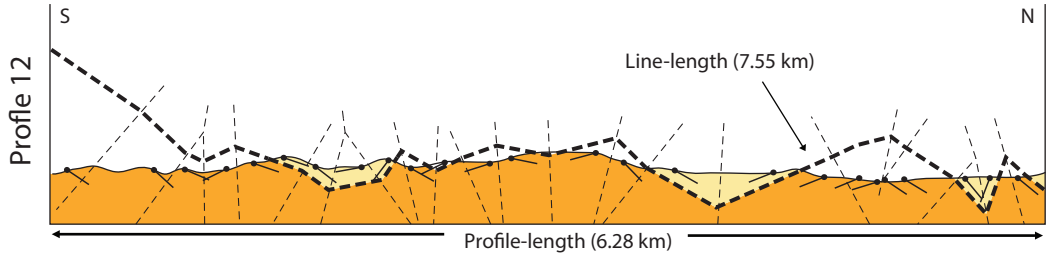

Lompoc - Santa Rosa Fold Belt; Profiles 13 - 16

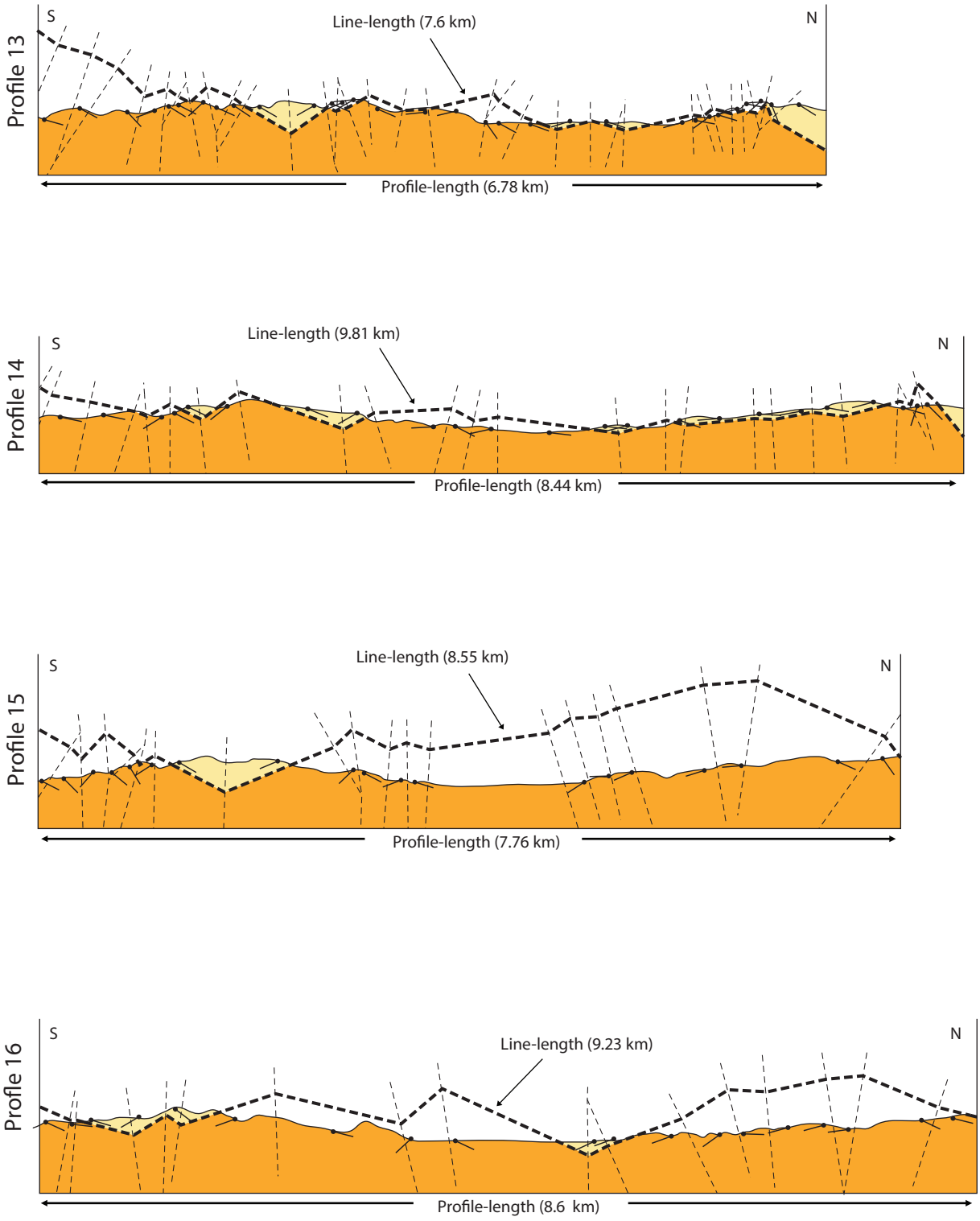

Lompoc - Santa Rosa Fold Belt; Profiles 17 - 19

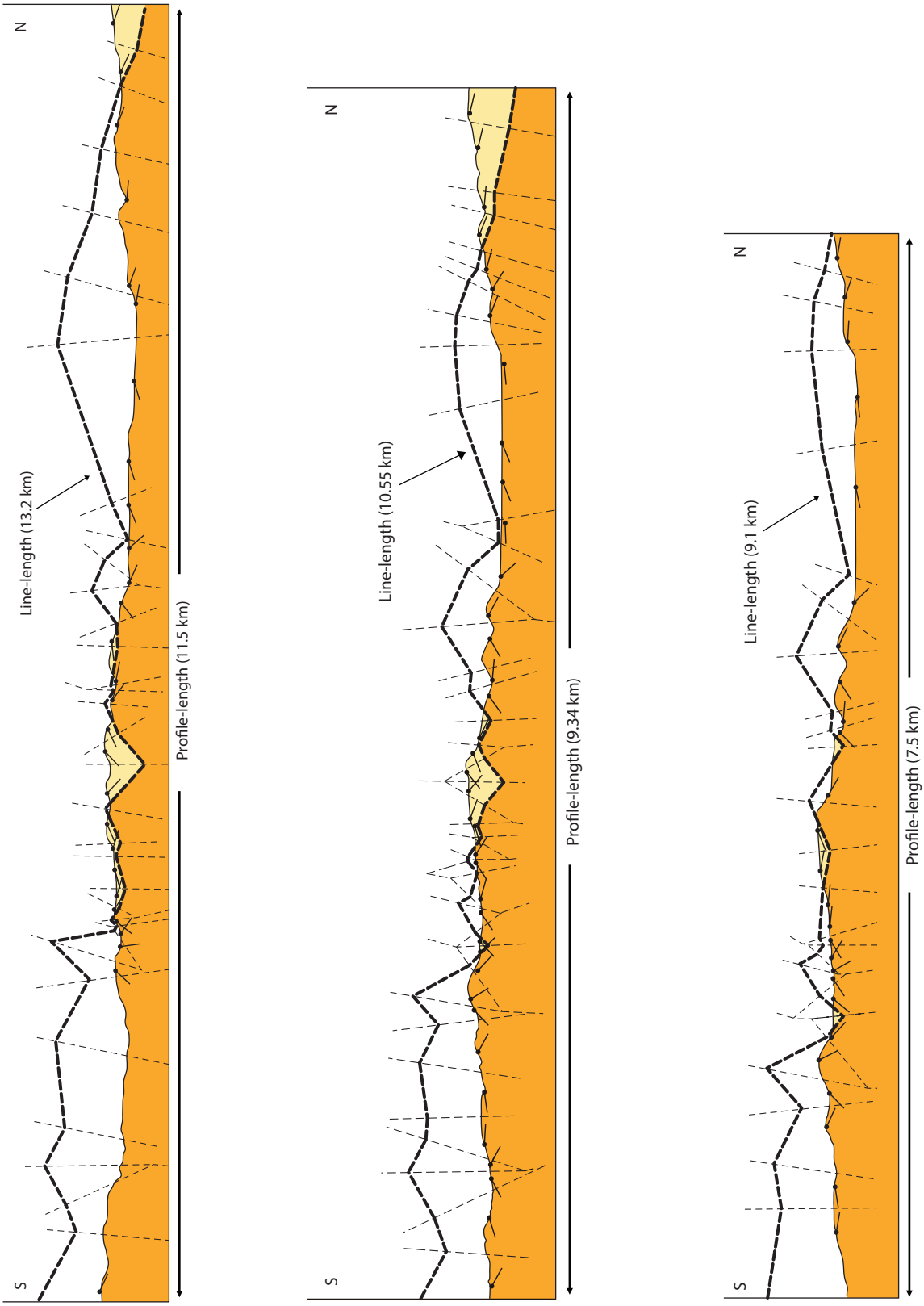

Lompoc Purisima Anticline Fold Belt; Profiles 20 - 24

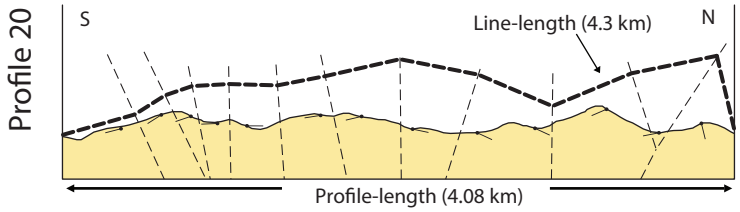

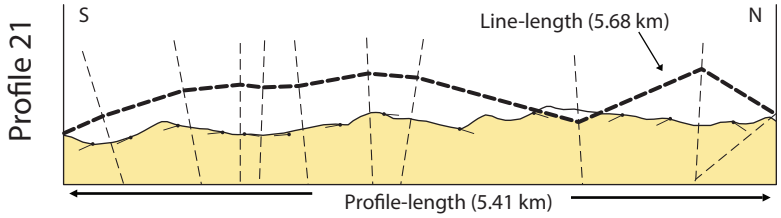

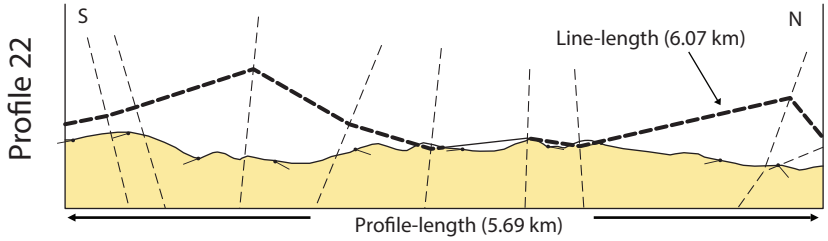

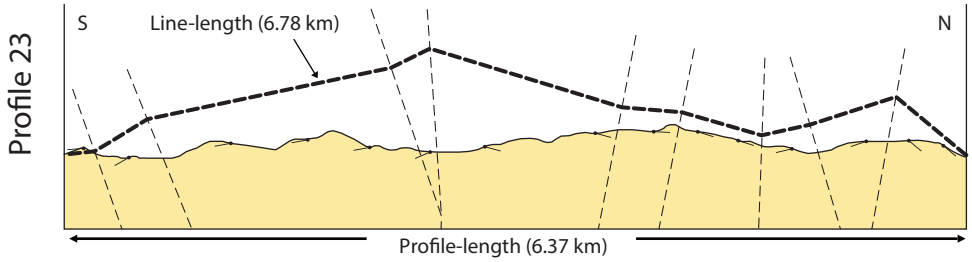

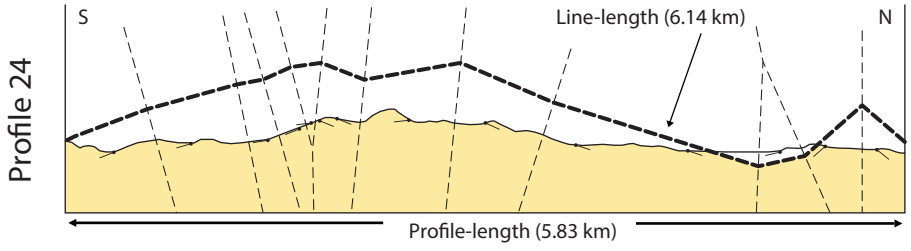

Lompoc Purisima Anticline Fold Belt; Profiles 25 - 28

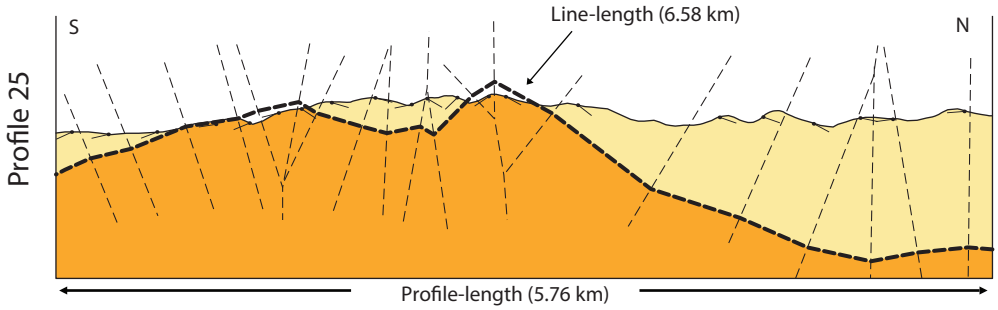

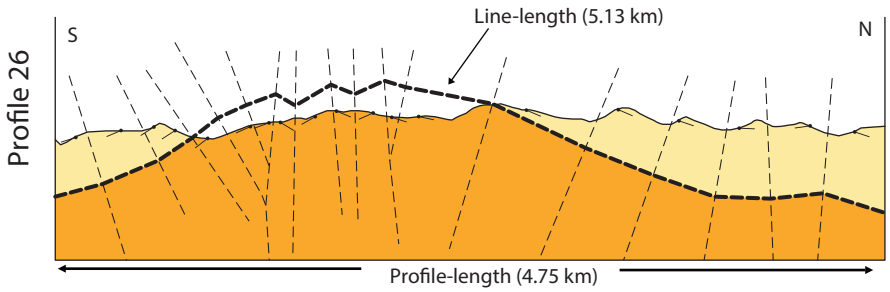

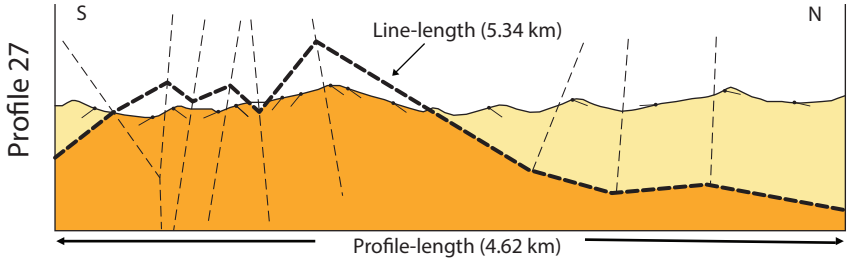

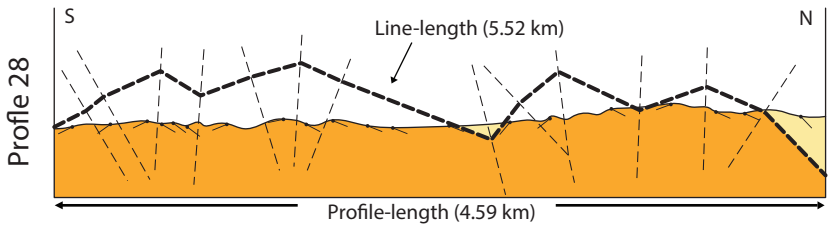

REFERENCES

REFERENCES

Behl, R. J., 1992, Chertification in the Monterey Formation of California and deep-sea sediments of the West Pacific, [Ph.D. thesis]: University of California, Santa Cruz.

Behl, R. J., 1999, Since Bramlette (1946), The Miocene Monterey Formation of California revisited: Geological Society of America Special Paper 338.

Behl, R.J., and Ingle, J.C., Jr., 1998, The Sisquoc/Foxen Boundary in the Santa Maria Basin, California: Sedimentary response to the new tectonic regime: US Geological Survey Bulletin, chapter V, p. v1-v16.

Blake, M.C., Campbell, R.H., Dibblee, T.W., Howell, D.G., Nilsen, T.H., Normark, W.R., Vedder, J.C., and Silver, E.A., 1978, Neogene basin formation in relation to plate-tectonic evolution of San Andreas Fault System, California: The American Association of Petroleum Geologists Bulletin, v. 62, no. 3, p. 344-372.

Carbonell, P.T., Dimieri, L.V., and Olivero, E.B., 2013, Evaluation of strain and structural style variations along the strike of the Fuegian thrust-fold belt front, Argentina: Andean Geology, v. 40, no. 3, p. 438-457.

Clark, D.H., Hall, N.T., Hamilton, D.H., and Heck, R.G., 1991, Structural analysis of late Neogene deformation in the central offshore Santa Maria Basin: Journal of Geophysical Research, v. 96, p. 6435-6458.

Cooper, M.A., 1983, The calculation of bulk strain in oblique and inclined balanced sections: Journal of Structural Geology, v. 5, p. 161-165.

Crouch, J., and Suppe, J., 1993, Late Cenozoic tectonic evolution of the Los Angeles basin and inner California borderland: A model for core complex-like crustal extension: Geological Society of America Bulletin, v. 105, p. 1415-1434.

Dahlstrom, C. D., 1969, Balanced cross sections: Canadian Journal of Earth Sciences., v.6, no. 743, p. 57-71.

Dibblee, T. W., Jr., 1950, Geology of southwestern Santa Barbara County: California Division of Mines Bulletin 150, 95 p.

Dibblee, T. W., Jr., 1982, Regional geology of the Transverse Ranges province of California, *in* Geology and Mineral Wealth of the California Transverse Ranges: New York, McGraw-Hill, p. 7-26.

Dibblee, T.W., Jr., and Ehrenspeck, H.E., 1988 a, Geologic map of the Lompoc and Surf quadrangles, Santa Barbara County, California: Dibblee Geological Foundation Map DF-20, scale 1:24,000.

Dibblee, T.W., Jr., and Ehrenspeck, H.E., 1988 b, Geologic map of the Solvang and Gaviota quadrangles, Santa Barbara County, California: Dibblee Geological Foundation Map DF-16, scale 1:24,000.

Dibblee, T.W., Jr., and Ehrenspeck, H.E., 1988 c, Geologic map of the Santa Rosa Hills and Secate quadrangles, Santa Barbara County, California: Dibblee Geological Foundation Map DF-17, scale 1:24,000.

Dibblee, T.W., Jr., and Ehrenspeck, H.E., 1988 d, Geologic map of the Lompoc Hills and Point Conception quadrangles, Santa Barbara County, California: Dibblee Geological Foundation Map DF-18, scale 1:24,000.

Dibblee, T.W., Jr., and Ehrenspeck, H.E., 1988 e, Geologic map of the Point Arguello and Tranquillon Mountain quadrangles, Santa Barbara County, California: Dibblee Geological Foundation Map DF-19, scale 1:24,000.

Dibblee, T.W., Jr., and Ehrenspeck, H.E., 1993 a, Geologic map of the Los Alamos quadrangle, Santa Barbara County, California: Dibblee Geological Foundation Map DF-46, scale 1:24,000.

Dibblee, T.W., Jr., and Ehrenspeck, H.E., 1993 b, Geologic map of the Zaca Creek quadrangle, Santa Barbara County, California: Dibblee Geological Foundation Map DF-45, scale 1:24,000.

Duebendorfer E.M., and Meyer L.M., 2002, Penetrative strain at shallow crustal levels: The role of pressure solution in accommodating regional shortening strain, Ventura basin, western Transverse Ranges, California: Geological Society of America Special Paper, v. 365, p. 295-314.

Engebretson D.C., and Cox A., 1985, Relative motions between oceanic and continental plates in the Pacific Basin: Journal of Geophysical Research, v. 89, p. 10,291-10,310.

Feigl, K.L., King, R.W., and Jordan, T.H., 1990, Geodetic measurement of tectonic deformation in the Santa Maria fold and thrust belt, California: Geophysical Research, v. 95, p. 2679-2699.

Fischer, M.P., and Jackson P.B., 1999, Stratigraphic controls on deformation patterns in fault-related folds: A detachment fold example from the Sierra Madre Oriental, northeast Mexico: Journal of Structural Geology, v. 21, p. 613-633.

Fossen H., 2016, Structural Geology: Cambridge, Cambridge University Press, 510 p.

Gross, M.R., Engelder, T., 1995, Strain accommodated by brittle failure in adjacent units of the Monterey formation, USA: scale effects and evidence for uniform displacement boundary conditions: Journal of Structural Geology, v. 17, p. 1303-1318.

Gross, M.R., Gutiérrez-Alonso, G., Bai, T., Collinsworth, K.B., Behl, R.J., 1997, Influence of mechanical stratigraphy and kinematics on fault scaling relations: Journal of Structural Geology, v. 19, p. 171-183.

Gutiérrez-Alonso, G., and Gross, M. R., 1997, Geometry of inverted faults and related folds in Monterey Formation: Implications for the structural evolution of the southern Santa Maria basin, California: Journal of Structural Geology, v. 19, no. 10, p. 1303-132.

Gutiérrez-Alonso, G., and Gross, M. R., 1999, Structures and mechanisms associated with development of a fold in the Cantabrian Zone thrust belt, NW Spain: Journal of Structural Geology, v. 21, no. 6, p. 653-670.

Hall, C. A., Jr., 1978, Origin and development of the Lompoc-Santa Maria pull-apart basin and its relation to the San Simeon-Hosgri strike-slip fault, western California, *in* San Gregorio-Hosgri Fault Zone, California: California Division of Mines Special Publication 137, p. 25-31.

Hall, C.A., Jr., 1982, Pre-Monterey subcrop and structure contour maps, western San Luis Obispo and Santa Barbara counties, south-central California: U.S. Geological Survey Miscellaneous Field Studies Map MF-1384, 6 sheets, scale 1:62,500, 28 p.

Hein, J.R., and Parrish, J.T., 1987, Distribution of siliceous deposits in space and time, *in* Siliceous Sedimentary Rock-Hosted Ores and Petroleum: New York, Van Nostrand Reinhold, p. 10-57.

Hogan, J.P., and Dunne, W.M., 2001, Calculation of shortening due to outcrop-scale deformation and its relation to regional deformation patterns: Journal of Structural Geology, v. 23, p. 1507-1529.

Hornafius, J.S., Luyendyk, B.P., Terres, R.R., and Kamerling, M.J., 1986, Timing and extent of Neogene tectonic rotation in the Western Transverse Ranges, California: Geological Society of America Bulletin, v. 97, p. 1476–1487.

Ingersoll, R. V., and Ernst, W. G., 1987, Cenozoic Basin Development of Coastal California (Rubey Volume VI): Englewood Cliffs, New Jersey, Prentice-Hall, 496 p.

Issacs, C. M., 1981, Outline of diagenesis in the Monterey Formation examined laterally along the Santa Barabara coast, California, *in* Guide to the Monterey Formation in the California Coastal Area, Ventura to San Luis Obispo: Menlo Park, Pacific Section American Association of Petroleum Geologists, p. 25-38.

Koyi, H. A., M. Sans, A. Teixell, J. Cotton, and H. Zeyen, 2003, The significance of penetrative strain in the restoration of shortened layers: Insights from sand models and the Spanish Pyrenees, *in* K. R. McClay, ed., Thrust Tectonics and Hydrocarbon Systems: American Association of Petroleum Geologists Memoir 82, p. 1-16.

Langenheim, V.E., Jachens, R.C., Graymer, R.W., Colgan, J.P., Wentworth, C.M., and Stanley, R.G., 2013, Fault geometry and cumulative offsets in the central Coast Ranges, California: Evidence for northward increasing slip along the San Gregorio - San Simeon - Hosgri fault: Lithosphere, v. 5, p. 29-48.

Laubach, S.E., Olson J.E., and Gross, M.R., 2009, Mechanical and fracture stratigraphy: American Association of Petroleum Geologists Bulletin, v. 93, no. 11, p. 1413–1426.

Luyendyk, B. P., and Hornafius, J. S., 1987, Neogene crustal rotations, fault slip, and basin development in southern California, *in* Ingersoll, R. V., and Ernst, W. G., eds., Cenozoic Basin Development of Coastal California (Rubey Volume VI): Englewood Cliffs, New Jersey, Prentice Hall, p. 259–283.

McCrory, P.A., Wilson, D.S., Ingle, J.C., Jr., and Stanley, R.G., 1995, Neogene Geohistory Analysis of Santa Maria Basin, California, and its Relationship to Transfer of Central California to the Pacific Plate: U.S. Geological Survey Bulletin 1995-J, 38 p.

McCrory, P.A., Wilson, D.S., and Stanley, R.G., 2008, Continuing evolution of the Pacific–Juan de Fuca–North America slab window system: A trench-ridge-transform example from the Pacific Rim: Tectonophysics v. 464, p. 30 - 42.

McQuarrie, N., and Davis, G.H., 2002, Crossing the several scales of strain-accomplishing mechanisms in the hinterland of the central Andean fold-thrust belt, Bolivia: Journal of Structural Geology, v. 24, p. 1587-1602.

Mitra, G., 1994, Strain variation in thrust sheets across the Sevier fold-and-thrust belt (Idaho-Utah-Wyoming): Implications for section restoration and wedge taper evolution: Journal of Structural Geology, v. 6, p.51–61.

Mitra, S., and Namson, J.S., 1989, Equal-area balancing: American Journal of Science, v. 289, p. 563-599.

Mount, V.S., and Suppe, J., 1987, State of stress near the San Andreas fault: Implications for wrench tectonics: Geology, v. 15, p. 1143-1146.

Mukul, M., 1999, Strain variation in fold-and-thrust belts: Implications for construction of retrodeformable models: Proceeding Indian Academy of Sciences (Earth and Planetary Sciences), v. 108, no. 3, p. 207-221.

Namson J. S., and Davis T. L., 1988 a, Seismically active fold and thrust belt in the San Joaquin Valley, central California: Geological Society Bulletin, v. 100, no. 2, p. 257-273.

Namson, J.S., and Davis, T.L., 1988 b, Structural transect of the Western Transverse Ranges, California: Implications for lithospheric kinematics and seismic risk evaluation: Geology, v. 16, p. 675–679.

Namson, J.S., and Davis, T. L., 1990, Late Cenozoic fold and thrust belt of the southern Coast Ranges and Santa Maria Basin, California: Bulletin of the American Association of Petroleum Geologists, v. 74, p. 467-492.

Nicholson, C., Sorlien, C., Atwater, T., Crowell, C., and Luyendyk, B., 1994, Microplate capture, rotation of the western Transverse Ranges, and initiation of the San Andreas transform as a low-angle fault system: Geology, v.22, p.491-495.

Onderdonk, N.W., 2005, Structures that accommodated differential vertical axis rotation of the western Transverse Ranges, California: Tectonics, v. 24, p. 1944 - 1994.

Ramsay, J.G., 1974, Development of chevron folds: Geological Society of America Bulletin v. 85, p. 1741-1754.

Ramsay, J.G., and Huber, M.I., 1983, The Techniques of Modern Structural Geology, Volume I: Strain Analysis: London, Academic Press.

Ramsay, J.G., and Huber, M.I., 1987, The Techniques of Modern Structural Geology, Volume II: Folds and Fractures: London, Academic Press.

Reed, R.D., and Hollister, J.S., 1936, Structural Evolution of Southern California: American Association of Petroleum Geologists, 157 p.

Smart, K. J., W. M. Dunne, and R. D. Krieg 1997, Roof sequence response to emplacement of the Wills Mountain duplex: The roles of forethrusting and scales of deformation: Journal of Structural Geology, v. 19, p. 1443-1459.

Snyder, W. S., 1987, Structure of the Monterey Formation: stratigraphic, diagenetic, and tectonic influences on style and timing, *in* Cenozoic Basin Development of Coastal California, Rubey Volume 6: Englewood Cliffs, New Jersey, Prentice Hall, p. 321-347.

Snyder, W.S., Brueckner, H.K., and Schweickert, R.A., 1983, Deformational styles in the Monterey Formation and other siliceous sedimentary rocks, *in* Stratigraphic, Tectonic, Thermal, and Diagenetic History of the Monterey Formation, Pismo and Huasna Basins: Society for Sedimentary Geology, no. 2, p. 151-171.

Sorlien, C., Kamerling, M. J., and Mayerson, D., 1999, Block rotation and termination of the Hosgri strike-slip fault, California, from three-dimensional map restoration: Geology, v. 27, no. 11, p. 1039-1042.

Suppe, J., 1980, A retrodeformable cross section of northern Taiwan: Proceeding Geological Society of China v. 23, 46-55.

Sylvester, A.G., and Darrow, A.C., 1979, Structure and neotectonics of the western Santa Ynez fault system in southern California: Tectonophysics, v. 52, p. 389–405.

Wilson, D.S., McCrory, P.A., and Stanley, R.G., 2005, Implications of volcanism in coastal California for the Neogene deformation history of western North America: Tectonics, v. 24, p 1-22.

Woodring, W. P., and Bramlette, M. N., 1950, Geology and Paleontology of the Santa Maria District, California: U.S. Geological Survey Professional Paper 222.

Zoback, M. D., et al., 1987, New evidence on the state of stress of the San Andreas fault System: Science, v. 258, p. 1105-1111.